Holocene Hydrographic Variations From the Baltic-North Sea Transitional Area (IODP Site M0059)

S. Ni[1,2] , N. B. Quintana Krupinski[1] , J. Groeneveld[3,4] , A. S. Fanget[5], M. E. Böttcher[6,7,8] , B. Liu[9], M. Lipka[6], K. L. Knudsen[5] , T. Naeraa[1], M.-S. Seidenkrantz[5] , and H. L. Filipsson[1]

[1]Department of Geology, Lund University, Lund, Sweden, [2]Centre for Environmental and Climate Research, Lund University, Lund, Sweden, [3]MARUM, Bremen University, Bremen, Germany, [4]Helmholtz Centre for Polar and Marine Research, Alfred Wegener Institute, Potsdam, Germany, [5]Palaeoceanography and Palaeoclimate Group, Interdisciplinary Centre for Climate Change (iClimate), Department of Geoscience, Aarhus University, Aarhus, Denmark, [6]Geochemistry and Isotope Biogeochemistry Group, Leibniz Institute for Baltic Sea Research (IOW), Warnemünde, Germany, [7]Marine Geochemistry, University of Greifswald, Greifswald, Germany, [8]Interdisciplinary Faculty, Department of Maritime Systems, University of Rostock, Rostock, Germany, [9]Alfred-Wegener-Institute, Helmholtz Centre for Polar and Marine Research, Section of Marine Geochemistry, Bremerhaven, Germany

Abstract Deoxygenation affects many continental shelf seas across the world today and results in increasing areas of hypoxia (dissolved oxygen concentration ([O_2]) <1.4 ml/L). The Baltic Sea is increasingly affected by deoxygenation. Deoxygenation correlates with other environmental variables such as changing water temperature and salinity and is directly linked to ongoing global climate change. To place the ongoing environmental changes into a larger context and to further understand the complex Baltic Sea history and its impact on North Atlantic climate, we investigated a high accumulation-rate brackish-marine sediment core from the Little Belt (Site M0059), Danish Straits, NW Europe, retrieved during the Integrated Ocean Drilling Program (IODP) Expedition 347. We combined benthic foraminiferal geochemistry, faunal assemblages, and pore water stable isotopes to reconstruct seawater conditions (e.g., oxygenation, temperature, and salinity) over the past 7.7 thousand years (ka). Bottom water salinity in the Little Belt reconstructed from modeled pore water oxygen isotope data increased between 7.7 and 7.5 ka BP as a consequence of the transition from freshwater to brackish-marine conditions. Salinity decreased gradually (from 30 to 24) from 4.1 to ~2.5 ka BP. By using the trace elemental composition (Mg/Ca, Mn/Ca, and Ba/Ca) and stable carbon and oxygen isotopes of foraminiferal species *Elphidium selseyensis* and *E. clavatum*, we identified that generally warming and hypoxia occurred between about 7.5 and 3.3 ka BP, approximately coinciding in time with the Holocene Thermal Maximum (HTM). These changes of bottom water conditions were coupled to the North Atlantic Oscillation (NAO) and relative sea level change.

Plain Language Summary The Baltic Sea is an intracontinental sea connected to the North Atlantic Ocean with large economic and societal values. It is sensitive to salinity and temperature changes and low oxygen conditions in the bottom water. The Little Belt is a transitional area between the central Baltic Sea and the North Sea. It is an ideal area to study the changes of freshwater outflow and saline water inflow and how the dynamics vary in relation to larger-scale climate changes. We have reconstructed past seawater conditions (e.g., temperature, salinity and oxygenation) in the Baltic by geochemically analyzing microfossil (foraminifera) shells. We analyzed the trace elemental concentration and stable oxygen and carbon isotopes in calcite shells of low-oxygen tolerant foraminiferal species as well as the benthic foraminiferal assemblages from a sediment core originating from the Little Belt covering the past 7,700 years. The salinity increased dramatically ~7,700–7,500 years ago and decreased ~4,100–2,500 years ago. Variation in bottom water oxygen content and bottom water temperature coincide. Our study highlights the benefit of using modern marine monitoring data together with a multiproxy approach to establish the link between local hydrographic conditions and regional climate changes and to explain how the environment has developed over time.

1. Introduction

The Baltic Sea is one of the world's largest semi-enclosed brackish water basins with a catchment area of 2.13×10^6 km^2, which is nearly 20% of the European continent (Nilsson, 2006). The catchment area has a

AGU
100
ADVANCING EARTH
AND SPACE SCIENCE

Paleoceanography and Paleoclimatology

10.1029/2019PA003722

Figure 1. Map of the southwestern Baltic Sea (basemap source: http://www.geomapapp.org). The position of IODP Site M0059 and long-term monthly monitoring hydrographic data (the Little Belt site, 55°00′N, 10°10′E) is shown as a red star. Water column samples taken during cruise MSM50 are shown as red open circles. Solid (surface water) and dashed (deep water) arrows indicate dominant current directions. The North Sea, Skagerrak, Kattegat, the three Danish Straits (Little Belt, Great Belt and Öresund), the Arkona Basin, the Drogden, and Darss Sills and the Baltic Sea are shown on the map.

total population of 85 million people across nine coastal and five upstream countries (International Council for the Exploration of the Sea (ICES), 2018). The sea experiences a considerable freshwater input from river runoff from the large surrounding catchment area (16,100 $m^3 s^{-1}$) but only a restricted inflow of saline water from the North Sea through the narrow Danish Straits (the Little Belt, the Great Belt, and the Öresund; Figure 1), making it a prime example of a restricted epi-continental sea. The restricted water exchange results in a permanent halocline that separates an upper layer of brackish water from more saline bottom waters. The permanent stratification in the deeper basins of the central Baltic plays an essential role in the bottom-water hypoxia and anoxia seen in many parts of the basin (e.g., Böttcher & Lepland, 2000). Here a strong halocline and a seasonal thermocline further weaken vertical circulation and ventilation of the bottom water (Lass & Matthäus, 2008). The salinity changes in the Baltic depend on the irregular inflow of North Sea water through the Danish Straits and the amount of freshwater runoff, which are in turn controlled by climatic factors in the Atlantic (Hänninen et al., 2000). The Baltic freshwater outflow into the Nordic Seas has a large potential influence on water mass transformation (Lambert et al., 2016, 2018; Winsor et al., 2001), by enhancing Polar Water outflow and suppressing Deep Water outflow (Lambert et al., 2018).

Strong stratification due to warming and water mass salinity contrasts can lead to bottom-water hypoxia in the Baltic Sea. Like many other continental shelf seas, it is frequently affected by hypoxia (Diaz & Rosenberg, 2008), which is further amplified with increased temperatures (Murray & Riley, 1969). Hypoxia is defined as <1.4 ml/L dissolved oxygen concentration ($[O_2]$) in the water. It has occurred intermittently, in particular in the deepest basins, in the Baltic Sea throughout the Holocene (Jilbert & Slomp, 2013; Kabel et al., 2012; van Wirdum et al., 2019), and the area of hypoxia has expanded sixfold from 1950 to 2000 CE (Carstensen et al., 2014). Baltic Sea hypoxic events have been steadily increasing with time and affect nutrient biogeochemical processes, ecosystem services, coastal habitats (Conley et al., 2009, 2011; Ning et al., 2018), and fisheries (Breitburg, 2002).

The Danish Straits hydrographically represent the transitional area between the Baltic Proper and the North Sea, and the salinity of these narrow straits is determined by the balance between the brackish water out-flows and the intermittent saline water inflows from the North Sea through the Kattegat and Skagerrak (Figure 1; Lass & Matthäus, 2008). The straits play an important role in the global ocean as they connect the largest brackish water system in Northern Europe to the Nordic Seas and the Atlantic Ocean. The straits are thus ideal sites to study the water exchange between the Baltic Sea and the North Sea and the role of such narrow gateways for water exchange in general. The flushing ratio between the three straits (the Little Belt, the Great Belt, and the Öresund) is 1:7:3 (Jacobsen, 1980; Helsinki Commission (HELCOM), 1986). The Little Belt is the smallest of the three Danish Straits (cross-section area: ~16 × 10³ km²; Hela, 1944), making it the most sensitive to changes in the hydrographical conditions in the Danish Straits. Therefore, the recon-struction of the hydrographic conditions in the Little Belt provides an indication of the conditions in the Danish Straits area as a whole.

Several studies have demonstrated that the North Atlantic Oscillation (NAO) (quantified by the NAO index) significantly influences the winter climate of the North Atlantic and northern European regions (e.g., Hurrell, 1995; Lu & Greatbatch, 2002; Trigo et al., 2002). Positive values of the NAO index are generally char-acterized by stronger westerly winds over northern Europe, usually causing the winter climate in northern Europe to be mild and wet. In contrast, a negative NAO index is associated with weaker westerly winds and more easterly/northeasterly winds, resulting in a cold and dry climate in northern Europe. In addition, var-iations in NAO drive sea-level changes (e.g., Marshall et al., 2001; Mehta et al., 2000; Wakelin et al., 2003), temperature (e.g., Hurrell, 1996; Hurrell et al., 2003), precipitation and freshwater fluxes (e.g., Hurrell, 1995; Hurrell et al., 2003). The wind field over Scandinavia controls the oscillations in water exchange in and out of the Baltic Sea and therefore also bottom water oxygenation. Westerly winds force more saline and oxyge-nated seawater from the North Sea-Skagerrak areas into the Baltic Sea, whereas easterly winds force brack-ish surface water out of the central Baltic Sea (Jakobsen & Ottavi, 1997; Lehmann et al., 2017). Major Baltic Inflows primarily occur between November and January and have shown very low frequencies during the summer months in the last century (Matthäus & Franck, 1992). During winter, strong easterly winds force the brackish surface water out of the Baltic Sea as a stronger Baltic Current and create a water level differ-ence between the Baltic Sea and the North Sea. When this is followed by a period of stronger westerly winds (i.e., during a positive NAO phase), it results in saline inflows into the Baltic Sea through the Little Belt and increasing water depth (i.e., sea-level rise) and bottom water salinity. Furthermore, bottom-water cooling and increased oxygen content are attributed to these major inflow events, particularly if they occur between January and April (Matthäus et al., 2008). The importance of the outflows from the Baltic (their strength and quantity) has also recently been highlighted as a very important factor for the living quality of the benthic environment in the Öresund-Danish Strait-Kattegat region (Charrieau et al., 2019).

The Baltic Sea has undergone six major environmental stages (lacustrine and marine) since the last degla-ciation (e.g., Andrén et al., 2011; Björck et al., 2008): the Baltic Ice Lake (~16–11.7 ka BP), the Yoldia Sea (11.7–10.7 ka BP), the Ancylus Lake (10.7–9.8 ka BP), the Initial Littorina Sea (9.8–8.5 ka BP), the Littorina Sea (8.5 ka BP to ~3 ka), and finally the present-day Baltic Sea. By ~10 ka BP the entire Baltic basin was deglaciated and sea-level rose above the straits' sills. The opening history of the three Danish Straits is complex, but it likely occurred between 9.3 and 8.1 ka BP (reviewed by Gyllencreutz et al., 2006). The marine ingression through the Great Belt occurred first ~9.0–8.7 ka BP and, through the Öresund slightly later (Gyllencreutz et al., 2006), with fully-brackish conditions reaching the southern Baltic at ~8.5 ka BP. The oldest dated marine shell from the Little Belt at IODP Site M0059 is from 7.7 ka BP, but brackish water conditions may already have been established between 8.6 and 8.3 ka BP (Bennike & Jensen, 2011). The long-term mean sea level in the Baltic Sea is mainly controlled by three factors: land uplift, eustatic sea level change, and water balance of the Baltic Sea (Johansson et al., 2001, 2003; Meier et al., 2004); this can further influence the water temperature and salinity in a relatively narrow and shal-low water environment like the Little Belt.

The general history of the Baltic is thus well known; however, it is essential to investigate further and in detail how temperature, salinity, and oxygen conditions have varied in the past in order to improve our understanding of the causes and consequences of environmental changes in the Baltic Sea. In particular, knowledge of these parameters will allow us to evaluate the overall stability of water exchange with the open ocean and evaluate the role of NAO on water exchange and hypoxia. This will provide a better insight into

the sensitivity of the Baltic Sea and other enclosed inland seas to external changes of the types expected to occur with current and future anthropogenic climate change.

To provide the strongest reconstruction of changes in temperature, salinity, and oxygenation in the Little Belt, we use a multiproxy approach based on benthic foraminifera, as summarized here. The occurrence and abundance of specific species of benthic foraminifera are indicators of bottom water conditions such as salinity and $[O_2]$ (e.g., Conradsen et al., 1994; Murray, 2006; Seidenkrantz, 1993). The oxygen isotopic composition of benthic foraminiferal calcite ($\delta^{18}O_c$) is a well established and the most widely used proxy for temperature and salinity of seawater (e.g., Elderfield et al., 2010; see Pearson, 2012 for review). In a semi-enclosed basin such as the Baltic Sea, it is possible to construct a relationship between $\delta^{18}O_c$ and salinity that represents a mixing line among different water masses (e.g., Fröhlich et al., 1988; Harwood et al., 2008). The mixing line can reveal salinity changes resulting from evaporation and precipitation, freshwater run-off and sea ice processes (e.g., LeGrande & Schmidt, 2006; Rohling & Cooke, 1999). Mg/Ca in benthic foraminifera is used as a bottom water temperature proxy (e.g., Elderfield et al., 2006; Filipsson et al., 2010; Groeneveld & Filipsson, 2013; Katz et al., 2010; Kristjánsdóttir et al., 2007). In addition, the Ba/Ca in foraminiferal calcite has been proposed as a proxy for dissolved Ba/Ca ratios in seawater (e.g., Hönisch et al., 2011; Lea & Boyle, 1989, 1991), which in coastal areas generally reflects the amount of freshwater run-off from land (e.g., Groeneveld et al., 2018). Therefore, Ba/Ca of foraminiferal calcite provides information on salinity, nutrients, and alkalinity distributions in seawater. Manganese is a redox-sensitive element, and its concentration in bottom and pore waters increases under hypoxic and anoxic conditions, which result in incorporation of more divalent Mn into the calcite lattice (Böttcher & Dietzel, 2010; Boyle, 1983). Mn/Ca in benthic foraminiferal calcite is being developed as a proxy for low oxygen conditions (e.g., Glock et al., 2012; Groeneveld & Filipsson, 2013; Groeneveld et al., 2018; McKay et al., 2015; Koho et al., 2015, 2017). Stable carbon isotopes in foraminifera ($\delta^{13}C_c$) are controlled by productivity, carbon cycling, and water mass exchanges, (e.g., Filipsson & Nordberg, 2010; Schmiedl & Mackensen, 2006). Thus, both Mn/Ca and $\delta^{13}C_c$ in benthic foraminifera can reflect past sea-water circulation and ventilation rates of the bottom water.

We apply this multiproxy approach to generate high-resolution reconstructions of Holocene bottom water conditions in the Little Belt by using the benthic foraminiferal geochemistry proxies and faunal assemblage analyses described above in a high-resolution sediment core from the Little Belt (Site M0059 from IODP Expedition 347) (Figure 1). A lower-resolution subset of some of these data (benthic foraminiferal faunal assemblages, Mg/Ca measured by solution-ICP-OES (Figure S1 in the supporting information), and foraminiferal $\delta^{18}O$) was published by Kotthoff et al. (2017). In the present study, we substantially increase the temporal resolution of the data sets (benthic foraminiferal faunal assemblages and carbon and oxygen isotopes) and we present new proxy variables (trace element/Ca measured by Laser Ablation Inductively Coupled Mass Spectrometry (LA-ICP-MS) and pore water oxygen isotopes ($\delta^{18}O_{pw}$)). We have selected samples spanning the time since our site became brackish-marine, that is, the last 7.7 kyr, which include major salinity changes and warming periods and, therefore, may provide a valuable analogue for future changes. The oldest part of the study period (~7.7 ka BP) includes the final portion of the transition from fresh-water conditions into the mid-Holocene brackish-marine Littorina Sea stage in the study area. We investigate the linkage between modern environmental conditions (i.e., temperature, salinity, and $[O_2]$) in the Little Belt and the NAO index and evaluate whether a similar linkage existed in the past. Our study's aims are to investigate the drivers and consequences of local environmental changes and to evaluate local environmental conditions (the Little Belt) as an indicator of regional climate changes (the Baltic Sea and the North Atlantic) over the past 7.7 kyr.

2. Modern Hydrographical Setting

Relatively low-salinity surface water exits the Baltic Sea through the Little Belt, while higher salinity inflows pass the main sills (Drogden and Darss Sills, Fischer & Matthäus, 1996) and become subsurface water when entering the Baltic Proper. Freshwater input in the Little Belt area is highest in May and June and lowest in January and February (Jakobsen, 1995). Long-term monthly monitoring hydrographic data covering the period CE 1975–2018 are available for the Little Belt (55°00′N, 10°10′E) from the Baltic Nest Institute, Stockholm University Baltic Sea Centre (Figure 2).
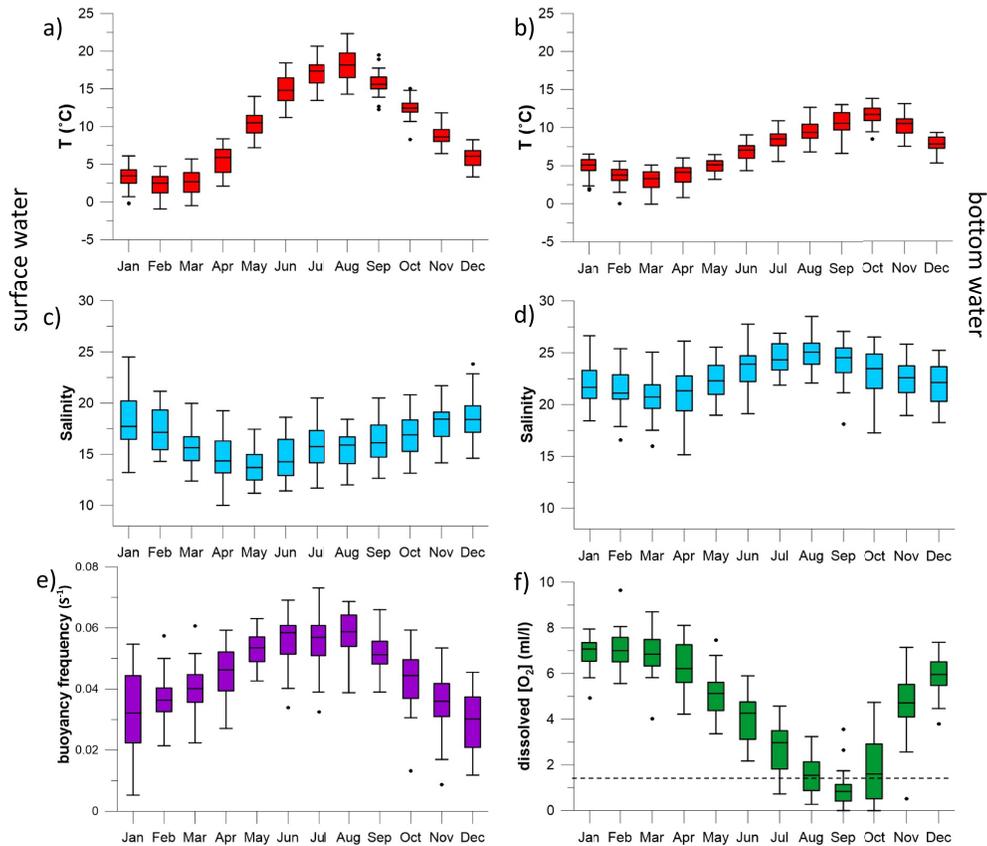
Figure 2. Little Belt monthly hydrographic monitoring data from Baltic Nest Institute, Stockholm University Baltic Sea Centre, 1975–2018, of (a) surface water (0–7 m) temperature, (b) bottom water (26–37 m) temperature, (c) surface water salinity and (d) bottom water salinity, (e) buoyancy frequency, and (f) bottom water dissolved $[O_2]$, the dashed line indicates hypoxic level ($[O_2]$ <1.4 ml/L). The dots indicate outliers with 1.5 Interquartile Rule.

2.1. Seasonal Variability in the Little Belt

The surface (0–7 m) and bottom waters (26–37 m) in the Little Belt area show strong seasonal variability (Figure 2). The average surface water temperature is ~17 °C in summer and 4 °C in winter. The monthly average bottom water temperature varied between 3 and 12 °C, and maximum and minimum temperatures occur in October and March, respectively. The temperature difference between surface and bottom water is largest between May and September (>5 °C). From November to February, the monthly average temperature in the bottom water is 1–2 °C higher than that in the surface water, whereas during the other months the bottom water is cooler than the surface water. The monthly average salinity is 14–19 in the surface water and 21–25 in the bottom water. The salinity difference between surface and bottom water is the largest (~9) from May to August. As an estimation of water column stability/stratification, we calculate the Brunt-Väisälä (buoyancy) frequency (N) following Godhe and McQuoid (2003),

$$N = \sqrt{-\frac{g}{\rho_1}\frac{\rho_2-\rho_1}{z_2-z_1}} \tag{1}$$

where g is gravitational acceleration (m s^{-2}), z is water depth (m), and ρ is density (kg m^{-3}). Depths used in the calculation were 5 and 30 m. Density is calculated from temperature, salinity, and pressure according to UNESCO (1981) and Massel (2015).

The average buoyancy frequency during the summer is 0.057 s^{-1}, whereas during the winter the buoyancy frequency is much lower (~0.032 s^{-1}). The large difference in salinity and thereby a strong halocline during summer time is the primary contributor to the high summer buoyancy frequency in the Little Belt. It indicates a stronger stratification in the water column, which may result in low dissolved $[O_2]$ in the bottom

water during summer. A strong pycnocline develops from May to September in the Little Belt, which also limits vertical mixing and promotes hypoxic bottom water. Seasonal hypoxia occurs in the bottom water and dissolved $[O_2]$ is typically lowest, <1.4 ml/l, in September, while the bottom water is generally fully oxygenated during the winter and spring (Figure 2).

3. Materials and Methods

3.1. Study Site, Lithology, Age model

Samples were collected during IODP Expedition 347 from Site M0059 (55°0.29′N, 10°6.49′E; 37.1 m water depth), located in the southern section of the Little Belt (Figure 1). IODP Expedition 347 obtained high-resolution sediment cores from the Little Belt covering the Holocene. The sedimentary sequence of Site M0059 has been divided into seven lithostratigraphic units (I–VII) (Andrén et al., 2015). Our study focuses on Subunit Ia (0 to 49.37 m composite depth (mcd)), which is the interval since the start of the Early to mid-Holocene brackish-marine Littorina Sea in the region. Subunit 1a is composed of black to greenish black, organic-rich clay with millimeter-scale lamination and minor bioturbation (Andrén et al., 2015).

We use the age-depth model of van Helmond et al. (2017) for the depth interval 0–48.6 mcd at Site M0059, which gives a calibrated age of −63 to 7437 year BP (where present is CE 1950). The age model is based on 16 radiocarbon (^{14}C) datings of intact bivalve specimens and bivalve fragments, and the sedimentation rate is generally steady with no abrupt changes in Subunit Ia (0.66 cm/year). In the bottom meter of Subunit Ia (48.6–49.37 mcd), ages were extrapolated linearly with the constant sedimentation rate of the interval above since no datable material was found.

We analyzed 127 depth intervals for foraminiferal $\delta^{18}O_c$ and $\delta^{13}C_c$, 37 depth intervals for trace elemental geochemistry (a total of 215 foraminiferal specimens) and 264 depth intervals for foraminiferal faunal assemblages at Site M0059. This resulted in an average age resolution of 56 years for $\delta^{18}O$ and $\delta^{13}C$ samples, 182 years for trace element samples, and 32 years for faunal assemblage samples. We analyzed 42 pore water samples for $\delta^{18}O$ and subsequently modeled the results to account for sediment compaction and pore water transport.

3.2. Benthic Foraminiferal Faunal Assemblages and Grain Size

We prepared foraminiferal samples following standard processing methods (Murray, 2006) via wet-sieving of 20 cm^3 sediment samples at mesh diameters 63, 100, and 1,000 μm. We used the 100 to 1,000 μm fraction for foraminiferal faunal assemblage analyses. For the sediment samples with a high concentration of mineral grains, we performed foraminiferal separation by using tetrachlorethylene (C_2Cl_4) with a specific density of 1.6 g cm^{-3} (for detailed description see Kotthoff et al., 2017). In each sample, we counted at least 300 foraminiferal specimens, identifying them to species level based on Feyling-Hanssen et al. (1971) and Feyling-Hanssen (1972), when possible. We assigned *Elphidium clavatum* Cushman and *Elphidium selseyensis* (Heron-Allen and Earland) to an *E. clavatum-selseyensis* complex due to the difficulties of reliably distinguishing the gradational morphologies (Groeneveld et al., 2018); however, our foraminiferal assemblage analyses show that *E. selseyensis* is the dominant of the two species. We calculated the relative abundance of each species, and if the relative abundance was >5% in at least one sample, we considered it a major species. We calculated the benthic foraminiferal concentrations as the number of individuals per cm^3 sediment and the Shannon index H by using PAST3 software to describe the faunal diversity. We obtained grain size data from the mass of the sand-sized fraction (>63 μm) from wet sieving during sediment sample preparation relative to the dried bulk sediment mass. Foraminiferal photographs (Figure S6) were prepared using the Leica Application Suite v. 4.12 and the Helicon Focus 7.0 stacking software.

3.3. Trace Element Ratios

For trace elemental analyses, we picked foraminifera from the size fraction 125–355 μm. We selected between three and seven specimens with complete final chambers from 37 depth intervals. We measured trace element ratios in the species *E. clavatum-selseyensis* complex on single foraminiferal chambers using LA-ICP-MS. Before trace element analysis, we briefly sonicated the foraminifera in MilliQ water and then methanol following Vetter et al. (2013).

A potential question in the study of any chemical proxy in marine sediments is the extent to which the primary "fossil" chemical signature was altered by postdepositional processes. This is particularly important to consider in hypoxic environments that are experiencing redox-related chemical reactions. We chose to use LA-ICP-MS analysis because it allows us to distinguish between trace metals associated with diagenetic coatings on shells (tests) and the primary calcium carbonate of the test. We conducted LA-ICP-MS analyses at Lund University using a Bruker Aurora Elite (quadrupole) ICP-MS and a 193 nm Cetac Analyte G2 excimer laser installed with a two volume HelEx2 sample cell. We used Helium as carrier gas (approximately 0.8 l/min) and combined this with Ar (approximately 0.95 l/min) downstream of the sample chamber. We tuned the instrument, using NIST612 to obtain high and stable signal counts on relevant elements, low oxide production (below 0.5% monitoring $^{238}U/^{238}U^{16}O$ and $^{232}Th/^{232}Th^{16}O$), and $^{232}Th/^{238}U$ ratios close to 1.

We ablated all foraminiferal tests from the outside toward the inside. Whenever possible, we selected the final (f), penultimate (f-1), and prepenultimate (f-2) chambers for ablation. We quantified element/Ca ratios using counts of the isotopes ^{24}Mg, ^{43}Ca, ^{55}Mn, ^{88}Sr, ^{27}Al, and ^{137}Ba. We calculated the element ratios based on averaging measured concentrations during each ablation after selecting the noncontaminated part of the ablation profile (removing the outer and inner layers) in order to avoid elevated element concentrations on the surface of the test (Figure S2). We used ^{43}Ca as the internal standard and NIST SRM 610 glass standard as the external calibration material (using established values from Jochum et al., 2011) because the NIST SRM 610 glass standard has been demonstrated to be more accurate and stable for elements with 193 nm laser than existing carbonate standards (Hathorne et al., 2008). We conducted laser ablation in manual mode and analyzed primary standards to correct for instrumental drift at the beginning of each sequence and throughout the run after roughly each 10 spot analyses. We measured baseline elemental levels before each analysis for minimum 30 s. We used NIST SRM 612 glass (Jochum et al., 2011) and calcium carbonate pellets of MACS-3 (Jochum et al., 2012), JCp-1, and JCt-1 (AIST Japan) as quality control material. We measured NIST SRM 610 and 612 glass standards at higher energy density (3 J/cm^2), whereas for all carbonate material we used 1 J/cm^2. We set the laser energy to 4 Hz and used a 30 × 30 μm spot size for both samples and standards. The changing of energy density (fluence) does not influence relevant element concentrations (Dueñas-Bohórquez et al., 2011). We converted raw counts to element concentrations (ppm) using the software package Igor Pro 6.37, Iolite v3.5.

In total, we used 402 ablation profiles on foraminiferal chambers for the trace element ratio calculations. All the ablation profiles we used fulfil the following criteria: (1) >12 sweeps (i.e., 3 s) of laser ablation, (2) averaged ^{27}Al concentrations of selected signal portions were below the limit of detection (the average of the background plus three times the standard error) in order to eliminate the spots with clay contamination. We observed that the trace element/calcium (TE/Ca) ratios of exterior and interior diagenetic coatings can be up to 40 times higher than the ratios of the original calcite (Figure S2). By omitting these coatings from the sample integration peak in data processing, Mg/Ca ratios of foraminiferal tests decrease by 30%, 72% for Mn/Ca and 29% for Ba/Ca. We first calculated mean values of trace element ratios of f, f-1, and f-2 chambers for each foraminiferal specimen and then calculated the median values of foraminiferal specimens at each depth interval with standard error.

We employed the Mg/Ca-temperature calibration established for *Melonis barleeanus* (Williamson) for semi-quantitative temperature reconstruction (Kristjánsdóttir et al., 2007):

$$T\ (°C) = \ln\left[Mg/Ca\ (mmol/mol)/0.658\pm0.07\right]/0.137\pm0.020 \qquad (2)$$

following Kotthoff et al. (2017) and Groeneveld et al. (2018). We did not apply the *E. clavatum* calibration of Barrientos et al. (2018) as it only covers the temperature range −2–0.5 °C and therefore is well outside of the range of temperatures expected at our study site. It should be noted that using a temperature calculation created for a different species than the one on which analyses are performed introduces some uncertainty.

3.4. Stable Oxygen and Carbon Isotopes in Foraminifera

We measured $\delta^{18}O_c$ and $\delta^{13}C_c$ on 124 samples (10–20 pooled specimens from the 100–1000 μm fraction) of the *E. clavatum-selseyensis* complex using a Thermo Finnigan MAT 251 gas isotope ratio mass spectrometer at MARUM, Bremen University, Germany. We express stable isotope values in per mil (‰) relative to the VSMOW and V-PDB standards in δ notation. We monitored accuracy and reproducibility by replicate

analysis of the in-house standard (Solnhofen limestone) calibrated to NBS19, and one standard deviation of this in-house standard is $\pm 0.03\permil$ for $\delta^{13}C_c$ and $\pm 0.06\permil$ for $\delta^{18}O_c$.

3.5. Oxygen Isotopes in Sea Water and Pore Water ($\delta^{18}O_{pw}$)

Forty-seven water column samples were collected during cruise MSM-50 of the RV *Maria S. Merian* in 2016 on a transect between the Skagerrak and the southern Baltic Sea (Bathmann et al., 2017) to establish the salinity-oxygen isotope covariation in modern waters within the North Sea-Baltic Sea transition. Water samples were taken at each station at three water depths (surface, middle and bottom) covering water depths between 1.3 and 379.1 m.

Water sampling took place using a Seabird SBE911plus CTD on an SBE-32 multiwater sampler equipped with 24 (10 l) Niskin bottles. Temperature and conductivity were measured with SBE-3plus and SBE-4C sensors, respectively (von Bröckel et al., 2018). Interstitial and pelagic water samples were stored in glass vials after on-board sampling until further processing in the IOW laboratory.

Pore water was extracted from the sediment immediately after recovery, using either rhizon samplers or squeezers, and subsampled under inert gas for stable water isotopes and further hydrochemical analyses according to standard IODP procedures (Andrén et al., 2015; Egger et al., 2017).

All stable oxygen isotope measurements ($\delta^{18}O$) were conducted by means of cavity ring-down spectroscopy (Picarro L2140-i) at the Leibniz Institute for Baltic Sea Research (IOW), with a reproducibility of better than $\pm 0.05\permil$ (1 standard deviation; Böttcher et al., 2014). Results are presented in the δ notation versus the international V-SMOW standard, using the IAEA standards VSMOW, SLAP, GISP, and USGS48, besides in-house standards, to scale the isotope measurements.

3.6. Pore Water Oxygen Isotope Modeling ($\delta^{18}O_{mpw}$)

We modeled advection and diffusion of pore water constituents since time of burial, as shown by $H_2^{18}O$, using a one-dimensional diffusion/advection equation under steady compaction (Berner, 1980; Boudreau, 1997):

$$\frac{dH_2^{18}O}{dt} = \frac{1}{\phi}\frac{\partial}{\partial z}\left(\frac{\phi D_0}{\tau^2}\cdot\frac{\partial H_2^{18}O}{\partial z}\right) - \frac{\omega_\infty \phi_\infty}{\phi}\frac{\partial H_2^{18}O}{\partial z} \tag{3}$$

where z is the depth, t is the time, ϕ is the porosity, τ^2 is the tortuosity, ω_∞ is the sedimentation velocity at depth, and D_0 is the molecular diffusion coefficient of $H_2^{18}O$. We calculated porosity as a function of depth (z),

$$\phi(z) = \phi_\infty + (\phi_0 - \phi_\infty)e^{-z/Y} \tag{4}$$

where ϕ_0 is the porosity at the water-sediment interface and ϕ_∞ is the depth below which porosity does not change. Y is the porosity e-folding distance. By fitting the measured porosity data in Site M0059, we get $\phi_\infty = 0.63$, $\phi_0 = 0.90$, and $Y = 50$ m. We used the mean sedimentation rate ω_∞ of 6.6 mm year^{-1} from the M0059 age model of van Helmond et al. (2017). We used the function of tortuosity from Boudreau (1996),

$$\tau^2 = 1 - 2ln\phi \tag{5}$$

We calculated the molecular diffusion coefficient of $H_2^{18}O$ as a function of temperature by using the equation given in Boudreau (1997),

$$logD_0 = a_1 + a_2\frac{1000}{T+273} + a_3\left(\frac{1000}{T+273}\right)^2 \tag{6}$$

where T is the temperature. The mean temperature was around 8 °C based on the multiproxy-based reconstruction of paleotemperature, paleosalinity, and paleoecosystem changes from the Little Belt (Site M0059) over the past ~8,000 years (Kotthoff et al., 2017). With $a_1 = 4.2355605$, $a_2 = 0.1642818$, $a_3 = -0.3525408$, and averaged temperature 8 °C, we get $D_0 = 0.0413$ m^2/year. The parameters of porosity, temperature, and sedimentation rate used in the model are slightly different from those used by Egger et al. (2017).
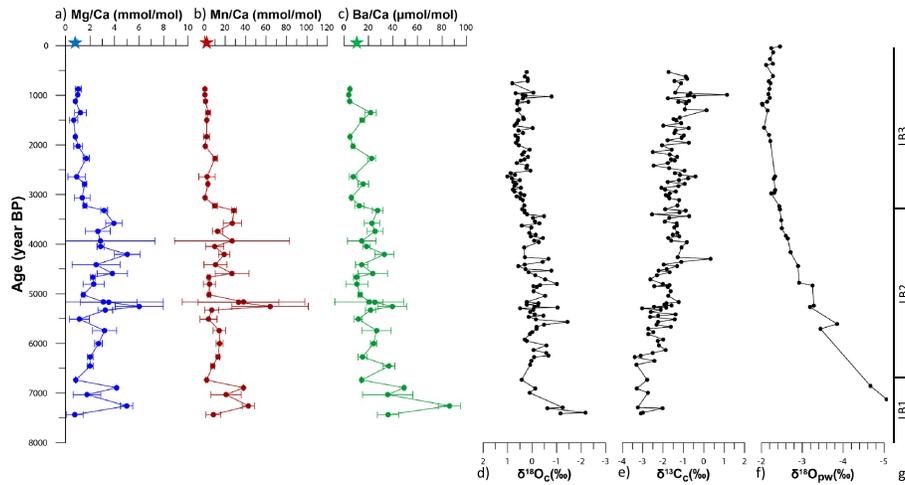
Figure 3. Trace element/Ca: (a) Mg/Ca, (b) Mn/Ca, (c) Ba/Ca, and stable isotopes: (d) $\delta^{18}O$ and (e) $\delta^{13}C$ measured on foraminifera of *E. clavatum-selseyensis* complex, (f) measured pore water $\delta^{18}O$ over the past 7.5 kyr, (g) local zones (LB1-3) based on foraminiferal geochemistry. Each trace element (TE) data point represents the median value of several foraminiferal individuals at each depth. The error bars of TE/Ca ratios represent one standard error (SE). The stars indicate modern typical values of TE in *E. clavatum-selseyensis* complex from the southern Baltic Sea (Groeneveld et al., 2018).

We solved the differential equation (equation (3)) by finite difference scheme. We set the sediment column height to 50 m and the duration of the diffusion/advection simulation to 7.2 kyr. We assumed the initial vertical geochemical profile to be homogeneous $\delta^{18}O_{fw} = -12$ at the freshwater lake period all along the length domain. We forced the model top boundary condition with the time evolution of the water-sediment interface concentration using the tracer of $\delta^{18}O(t)$. At each time step, the model accounted for the new boundary condition at the top and vertically advected and diffused the tracer ($\delta^{18}O$), according to equation (3). $\delta^{18}O(t)$ increased linearly from $\delta^{18}O_{fw} = -12$ to maximum $\delta^{18}O_{max} = -1$ within 400 years (7.7 to $\sim$7.3 ka BP) and remained at $\delta^{18}O_{max}$ for another 3,300 years (until 4.0 ka BP). Then $\delta^{18}O(t)$ gradually decreased to the current $\delta^{18}O_{curr} = -2.3$ within 2.9 kyr (4.0 to 1.7 ka BP) and kept at $\delta^{18}O_{curr}$ up to 0.5 ka BP. We did not apply a diffusive boundary condition at the model bottom boundary.

We applied modeled pore water $\delta^{18}O$ data to the paleotemperature equation (Shackleton, 1974):

$$T\ (^{\circ}C) = 16.9\ -\ 4.0 \times \left(\delta^{18}O_{c,V-PDB}\ - \ \left(\delta^{18}O_{mpw,SMOW}\ -\ 0.27 \right) \right) \tag{7}$$

in order to solve for the influence of temperature on oxygen isotope fractionation in foraminiferal calcite.

3.7. Statistical Analyses

Because the sampling depth intervals in this study differ for each proxy, we interpolated between data points in higher-resolution datasets in order to evaluate correlation with lower-resolution datasets. All correlation analyses of two parameters use measured data and interpolated data (linear interpolation) with same age intervals. We applied the Pearson's correlation test and t test and considered $P < 0.05$ as significant.

4. Results

We have subdivided the Holocene record of the Little Belt (LB) into three local zones (LB1-3; Figure 3) based on our proxy records: LB1 (7.7–6.8 ka BP) is characterized by high and variable Mg/Ca and Mn/Ca, decreasing Ba/Ca values, highly variable occurrences of *Elphidium incertum* (Williamson), and increasing $\delta^{18}O_c$ and $\delta^{18}O_{pw}$; LB2 (6.8–3.3 ka BP) is distinguished by higher trace element/Ca, and more negative $\delta^{18}O_c$, and a continued increase in $\delta^{18}O_{pw}$; LB3 (3.3 ka BP to present) is characterized by lower and more stable trace element/Ca, $\delta^{18}O_c$, and $\delta^{18}O_{pw}$.

4.1. Benthic Foraminiferal Trace Element/Ca

The Mg/Ca ranged from 0.8 ± 0.7 to 6.0 ± 2.0 mmol/mol through the record (7.5–0.8 ka BP) (Figure 3a). The values were relatively higher and more variable during LB1 and LB2, with an average value of 2.9 ± 1.3
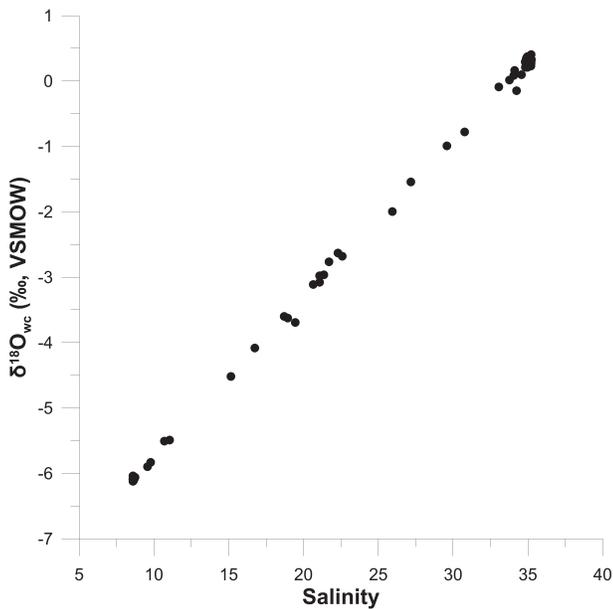
Figure 4. Covariation of the oxygen isotope composition of the modern water column ($\delta^{18}O_{wc}$) as a function of salinity on a transect between the Skagerrak and the southern Baltic Sea (cruise MSM 50). Sampling sites are shown in Figure 1.

mmol/mol in this period, and the highest values around 5.3 ka BP (6.0 ± 2.0 mmol/mol). There were two periods with relatively high Mg/Ca values, that is, 7.3–6.8 and 5.7–3.3 ka BP. During LB3, the Mg/Ca was lower and varied less, in the range of 0.7 ± 0.4 to 1.7 ± 0.3 mmol/mol.

During LB1 and LB2, the Mn/Ca values were more variable and much higher than values established in modern calibrations (up to 15 times higher than values in, e.g., Groeneveld et al., 2018; Figure 3b) and only occasionally lower than 5 mmol/mol. Two periods show increasing Mn/Ca values: 6.7–5.7 and 4.7–3.3 ka BP, when Mn/Ca values increased from 1.9 ± 0.7 to 14.3 ± 6.0 mmol/mol and 4.0 ± 1.4 to 28.6 ± 2.4 mmol/mol, respectively. Mn/Ca values were relatively stable and low during the last ~2 kyr, varying between 0.2 ± 0.1-3.4 ± 2.5 mmol/mol.

Ba/Ca data show three clear phases: an initial rapid decrease during LB1, a moderate phase during LB2, and then the lowest values during LB3. Ba/Ca values vary from 3.9 ± 0.0 to 39.5 ± 11.8 μmol/mol from 7 ka BP to present (Figure 3c).

4.2. Benthic Foraminiferal Stable Oxygen and Carbon Isotopes

Foraminiferal $\delta^{18}O$ and $\delta^{13}C$ values in the Little Belt became more positive through time, showing a range from −2.2‰ to 1.0‰ for $\delta^{18}O_c$ and −3.4‰ to 1.1‰ for $\delta^{13}C_c$ (Figures 3d and 3e). The $\delta^{18}O_c$ values in LB3 are less variable and more positive than the values during LB1 and LB2. The most rapid permanent change in $\delta^{18}O_c$ occurred during LB1, when $\delta^{18}O_c$ increased from −2.2‰ to 0.4‰. The average value was ~−0.2‰ in LB2, varying from −1.4‰ to 0.6‰. There was a steady increase in $\delta^{18}O_c$ from 3.4 ka to 2.5 ka BP. After 2.5 ka BP, $\delta^{18}O_c$ became more stable, ranging from −0.8‰ to 0.8‰ with an average value of 0.4‰. In general, $\delta^{13}C_c$ increased throughout the record. During the first 3 kyr, the $\delta^{13}C_c$ values show a clear increasing trend from −3.4‰ to −1.1‰. From around 4 ka BP to present, the increase of $\delta^{13}C_c$ slowed down, and the average value is −1.3‰.

4.3. Water Column and Pore Water Oxygen Isotopes

In the modern water column of the North Sea-Baltic Sea transition (Figure 1), we determined a linear covariation between salinity and the oxygen isotope composition of sea water ($\delta^{18}O_{wc}$) (Figure 4):

$$\delta^{18}O_{wc} = 0.24 \times salinity - 8.14 \; (r^2 = 0.999; n = 48) \tag{8}$$

The salinity of the water column varied between 35.2 and 20.6 from the Skagerrak to the Kattegat (sampling station numbers 014–024 in Figure 1), and $\delta^{18}O_{wc}$ shows a range of −3.1‰–0.4‰. In the Baltic Sea (station numbers 025–030) the salinity was 21.4–8.6, and the $\delta^{18}O_{wc}$ varied in a range between −6.1‰ and −3.0‰.

Pore water oxygen isotopes ($\delta^{18}O_{pw}$; Figure 3f) show a trend of increasing $\delta^{18}O_{pw}$ values with time from −5‰ to −2‰ VSMOW, with the most rapid increase between 7.5 and 5.0 ka BP, a slower increase in LB2, and relatively stable values in LB3. The modeled pore water oxygen isotopes ($\delta^{18}O_{mpw}$) present a very rapid increase between 7.7 and 7.5 ka BP from −2.5‰ to −1.0‰ and reached a relatively high, stable value of −1.0‰ in the following 3.4 kyr. Between 4.1 and 3.0 ka BP, $\delta^{18}O_{mpw}$ rapidly decreased from −1.0‰ to −2.1‰ and then remained fairly stable around −2.2‰ ± 0.1‰ in the most recent ~2.5 ka.

We calculated the $\delta^{18}O$-based salinity by using the linear correlation between salinity and $\delta^{18}O_{wc}$ we established in equation (8).

4.4. Benthic Foraminiferal Faunal Assemblages and Grain Size

In general, the foraminiferal fauna is dominated by the *E. clavatum-selseyensis* complex and the faunal assemblage diversity of the Little Belt is relatively low throughout the time interval (Figure 5). Between 7.5 ka and 6.0 ka BP, the fauna consisted of a more diverse assemblage (Shannon H index = ~0.8) consistently dominated by *Elphidium incertum* (Williamson) and *E. clavatum-selseyensis* complex (>90%).
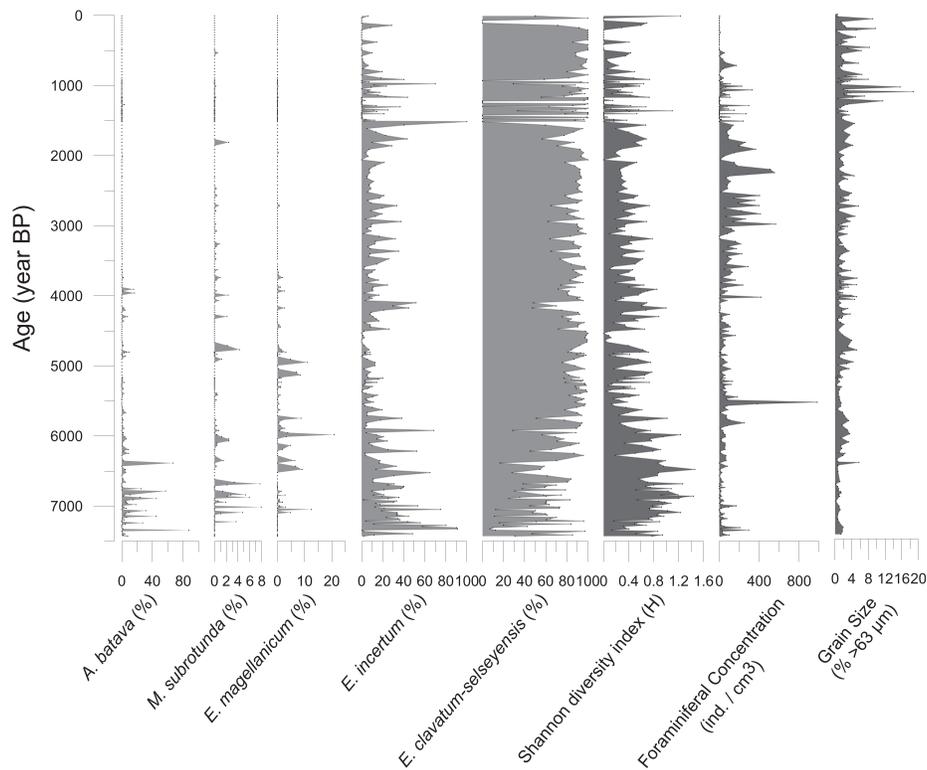
Figure 5. Faunal assemblage data showing relative abundances (%) of the foraminiferal major species (>5% in at least five samples), benthic foraminiferal diversity (Shannon H index) and concentration, as well as sediment grain size (sand weight %). Note the different scales on the *x* axes (Foraminiferal major species with >5% relative abundances in at least one sample are shown in Figure S5, light microscope images of five major species are shown in Figure S6).

During this period, *Ammonia batava* (Hofker) (previously assigned to *Ammonia beccarii* by Kotthoff et al. (2017) but here reassigned to *A. batava* following Hayward et al. (2019)) occasionally became a dominant species, and *Elphidium magellanicum* (Heron-Allen & Earland) and *Miliolinella subrotunda* (Montagu) had relatively higher concentrations (>5%), but overall the concentration of specimens was low (~37 individuals per cm^3). After approximately 6 ka BP, the faunal assemblage changed, and the diversity decreased around 5.5 ka BP (Shannon H index = ~0.3), indicating a gradual environmental change. Total abundance of benthic foraminifera generally increased over time (except for the last ~500 years), and they were most abundant around 5.5 ka BP and from 4.0 ka to 0.5 ka BP, potentially caused by a more preferable environment or better preservation. The percentage of sand grains of sediment generally increased through time, and in particular, the sediment became sandier after 1.3 ka BP.

5. Discussion

5.1. Salinity and Temperature Changes in the Little Belt

Foraminiferal calcite δ^{18}O$_c$ is generally influenced by two parameters, that is, temperature and seawater oxygen isotope composition, which is correlated with salinity (Figure 5). Salinity changes are caused by the combined effects of evaporation, precipitation and runoff, and mixing processes are coupled with changes in seawater δ^{18}O$_w$ (Gat, 1996; Harwood et al., 2008). The mixing line determined in our study between salinity and modern water column δ^{18}O$_{wc}$ is similar to that of Fröhlich et al. (1988): Salinity = (δ^{18}O$_{wc,\ SMOW}$ + 8.91)/0.272, but with the benefit of a wider salinity range in our study (8–35). Water masses in the Little Belt, which originate in the Skagerrak, the North Atlantic and the central Baltic Sea, are mixed and renewed constantly. Due to the complex hydrographic setting of the Danish Straits, it is complicated to distinguish the respective influence of temperature and salinity on δ^{18}O$_c$ values, and therefore, estimating paleosalinity from δ^{18}O$_c$ records is not straightforward. However, with δ^{18}O$_{wc}$ and δ^{18}O$_{pw}$ data, it becomes possible to calculate bottom water salinity according to a mixing line among different water masses and to calculate
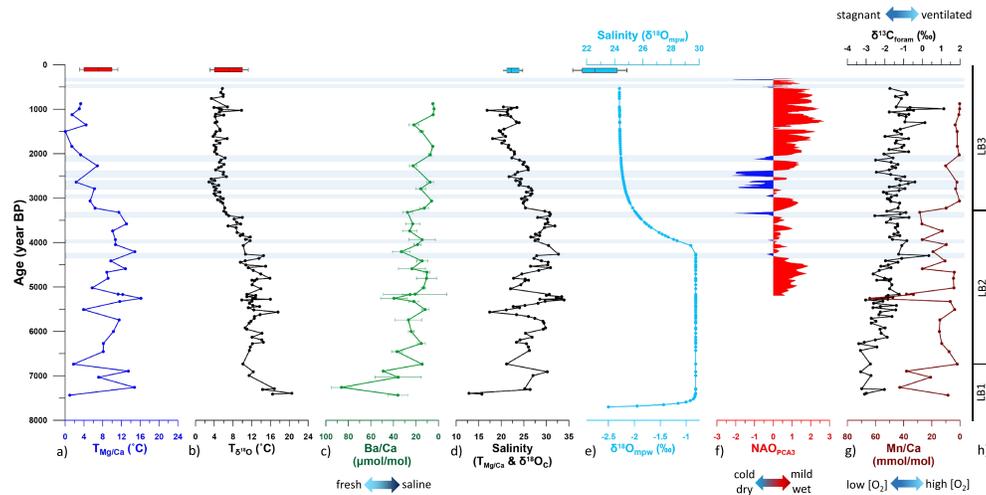
Figure 6. Temperature, salinity, and oxygen content proxies and calculations from pore water and foraminiferal results. Calculated bottom water temperature (BWT) based on foraminiferal calcite: (a) Mg/Ca and (b) $\delta^{18}O$ (using $\delta^{18}O_c$ and $\delta^{18}O_{mpw}$); salinity proxies from foraminiferal calcite: (c) foraminiferal Ba/Ca (μmol/mol); reconstructed bottom water salinity: (d) absolute salinity calculated from $T_{Mg/Ca}$ and $\delta^{18}O_c$, (e) modeled bottom water changes before modification via advection and diffusion processes in the sediment column ($\delta^{18}O_{mpw}$) and the calculated salinity based on pore water $\delta^{18}O_{mpw}$ (section 2.6); (f) Inferred NAO circulation patterns NAO_{PCA3} (modified from Olsen et al., 2012); oxygenation proxies from foraminiferal calcite: (g) foraminiferal calcite $\delta^{18}C_c$ (‰-V-PDB) and Mn/Ca (mmol/mol); (h) local zones (LB 1-3) based on foraminiferal trace element and stable isotope data and reconstructed temperature and salinity. The blue shadow indicates negative phases of NAO. The red and blue box charts on top of (a), (b), (d), and (e) show the modern temperature and salinity variation range, respectively. Note that x axes of Ba/Ca and Mn/Ca are reversed.

bottom water temperature, considering oxygen isotope fractionation in equilibrium between $\delta^{18}O_c$ and seawater.

We use two types of geochemical salinity proxies from Site M0059. One is the modeling of advection and diffusion of the pore water $\delta^{18}O$ ($\delta^{18}O_{pw}$), which shows that salinity increased from ~24 to 30 during the time interval 7.7–7.5 ka BP (Figure 6e). From 7.5 to 4.1 ka BP, the $\delta^{18}O_{pw}$ indicates bottom-water salinity environments of ~30 in the Little Belt. The bottom-water salinity decreased from ~30 to ~24 in the time interval from ~4.1 to ~2.5 ka BP (Figure 6e). The other paleosalinity proxy type is the foraminiferal salinity proxies, Ba/Ca and $\delta^{18}O_c$, which show an initial salinity increase during LB1, subsequently followed by a higher bottom-water salinity stage during LB2. The salinity continued to increase during LB3. Of these two groups of paleosalinity proxies, the $\delta^{18}O_{mpw}$ reconstructed salinity is similar to the salinity trends of the past 8 kyr estimated by Gustafsson and Westman (2002), who found that the salinity of the Baltic Sea reached Holocene maximum values between 6 and 4 ka BP and decreased after ~4 ka BP reaching modern day salinity after ~2 ka BP.

We calculated bottom water temperature using two independent methods: (1) by combining $\delta^{18}O_c$ and $\delta^{18}O_{pw}$ data following Shackleton (1974) and (2) by using Mg/Ca and the calibration of Kristjánsdóttir et al. (2007). Both Mg/Ca-based and $\delta^{18}O$-based bottom water temperature reconstructions (Figures 6a and 6b) provide similar trends in the Little Belt over the past 7.5 kyr, though absolute values are generally somewhat higher for the $\delta^{18}O$-based results (average ~1 °C higher) than for the Mg/Ca-based results. In general, $\delta^{18}O$-based bottom-water temperature reconstruction ($T_{\delta18O}$) is less variable than Mg/Ca-based bottom water temperature reconstruction ($T_{Mg/Ca}$). Both temperature proxies give a large range of bottom water temperature values, varying between ~21 and 3 °C for $T_{\delta18O}$ and between ~16 and 0 °C for $T_{Mg/Ca}$ over the past 7.5 kyr, although this range is only slightly larger than present day bottom water variations throughout the year. The warming period from 7.5 to 4.1 ka BP coincides with the timing of the HTM as traditionally defined for the Baltic (between 8 and 4 ka BP, Sohlenius et al., 2001; Zillén et al., 2008), which is slightly longer than the typical timing of 7 to 6 ka BP in most of Europe (Renssen et al., 2012). The mean bottom water $T_{\delta18O}$ and $T_{Mg/Ca}$ during the time interval 6.5–4.1 ka BP were stable and warm at about 12.5 ± 1.7 °C and 10.3 ± 3.2 °C, respectively. This warm period was also characterized by more negative $\delta^{13}C$ values (Figure 6g). The negative $\delta^{13}C$ values of benthic foraminifera have also been found during both Medieval

and recent warm periods and may suggest high primary productivity (Filipsson & Nordberg, 2010; Polovodova Asteman et al., 2018).

The reconstructed temperature decrease after ~4.1 ka BP (Figures 6a and 6b) is associated with a salinity decrease, shown by our $\delta^{18}O_{mpw}$ and foraminiferal geochemistry salinity reconstructions (Figures 6d and 6e). Salinity and temperature remained at ~24 and ~6 °C ($T_{\delta18O}$) during the last ~2.5 kyr. These values are in the range of modern annual mean bottom water salinity and temperature (Figures 2b and 2d). The salinity decrease starting ~4.1 ka BP is not clearly observed in Ba/Ca. Instead, the Ba/Ca shows that the salinity increased slightly after ~4.1 ka BP, perhaps due to other factors controlling foraminiferal Ba/Ca such as nutrient supply, local freshwater source Ba/Ca variations and organic matter decomposition at the sea floor. The ostracod faunal assemblage also reflects a shallow brackish environment with reduced salinity after ~4 ka BP in the Little Belt (Stepanova et al., 2019). The salinity decrease between ~4.1 and 3 ka BP agrees with existing salinity reconstructions in the central parts of the Baltic Sea (e.g., Emeis et al., 2003; Ning et al., 2017).

Although the absolute temperature values of Mg/Ca-based and $\delta^{18}O$-based reconstructed bottom water temperature differ, both show a steady temperature decrease of ~7 °C from 4.1 to 2.5 ka BP. This coincides with the period of salinity decrease, indicating substantial environmental change. $T_{\delta18O}$ increased slightly around 2.5 ka BP, following the previous decrease, and became relatively less variable, with a mean $T_{\delta18O}$ value of 5.2 ± 1.2 °C. This is in the same range as modern bottom water temperature during winter or spring, which is known as the period when a majority of typical shallow-water foraminiferal calcification occurs (e.g., Gustafsson & Nordberg, 2001). Mean temperature from both proxies was lowest between 2.5 and 0.5 ka BP (3.0 ± 2.1 °C).

Based on equations (2), (7), and (8), we calculated the salinity from $T_{Mg/Ca}$ and $\delta^{18}O_c$ (Figure 6d), and the results broadly agree with $\delta^{18}O_{mpw}$-based salinity. During LB1, there was a rapid salinity increase followed by a relatively saline period (LB2). After a subsequent decrease in LB3, salinity reached the modern values at ~1.5 ka BP.

The true temperature variations may not be as large as indicated by the proxy reconstructions (~7 °C) (Figure 6). This could be attributed to at least one of the following reasons: (1) Decreased water depths in the Little Belt may have reduced warm Atlantic water inflows, such that the bottom water was replaced by cooler and fresher water from the Baltic Sea; (2) there were changes in seasonality of foraminiferal calcification, and the bottom water seasonal temperature difference can be up to ~7 °C as shown in modern oceanographic records (Figure 2b); (3) as species-specific temperature calibration equations for *E. clavatum-selseyensis* complex are lacking, the use of a calibration equation of another species may introduce larger variability; (4) the $T_{\delta18O}$ reconstruction also contains uncertainties from $\delta^{18}O_{pw}$ and $\delta^{18}O_{mpw}$. The modeled pore water profiles are not sensitive to the time when the salinity started to decrease (Figure S3d) but show some variation with different decay rates (Figure S3a). However, the time and decay rate affect the isotopic temperature change (Figure S3b). In this study, we set $\delta^{18}O_{max} = -1.0$ at 4.1 ka BP (Figure S3c). The error bar of $\delta^{18}O_{max}$ is ±0.5, which leads to a temperature uncertainty of 2 °C around 4.1 ka BP according to equation (7). Therefore, the temperature difference between 4.1 and 2.5 ka BP is around 7 ± 2 °C; and (5) a slight influence of diagenesis cannot be excluded. The laser ablation allows to avoid surface coatings in data processing but does not exclude diagenetic imprints present within the tests, for example, in pores (Figure S4).

The pattern of foraminiferal faunal assemblages also highlights the salinity changes at Site M0059. The species diversity decreased (Figure 3) when temperature and salinity changed dramatically in the first ~1 to 2 kyr of our record. *Ammonia batava* had relatively high frequencies from 7.5 to 6.3 ka BP, varying from 20% to 90%, indicating a relatively low salinity environments during this first millennium after the marine inundation of the southern Little Belt, as this species is typical of low salinity environments (Murray, 2006; Seidenkrantz, 1993). There is a significant inverse correlation between the *E. clavatum-selseyensis* complex and *E. incertum* ($r^2 = 0.94$, $p << 0.01$) throughout the record. From 7.5 to 5.5 ka BP, *A. batava*, *E. clavatum-selseyensis* complex and *E. incertum* alternatingly dominated the benthic foraminiferal fauna, presumably due to salinity variations during this period. From 5.5 ka BP to present (which includes the end of the HTM around ~4 ka BP), the diversity and the relative abundance of *E. incertum* decreased and the *E. clavatum-selseyensis* complex dominated the assemblage, presumably due to its high tolerance to relatively large variations in salinity (Charrieau et al., 2018; Murray, 2006). From 7.4 to 4.1 ka BP, freshwater indicators (i.e., diatoms, green algae, and ostracods) also rapidly decreased or disappeared (Andrén et al., 2015;

Stepanova et al., 2019). Increases in the abundance of *E. incertum* and in diversity likely indicates periods of saline influx.

In the Baltic Sea, the first large salinity increase in the present study interval was at the very end of the transitional stage (the Initial Littorina phase) between the fresh-water of the Ancylus Lake and the following brackish-marine Littorina Sea stage (9-7 ka BP, Zillén et al., 2008; Kotthoff et al., 2017; Stepanova et al., 2019), subsequently followed by a temperature rise. During the beginning of Littorina Sea stage (~7.5–4.5 ka BP), the southern Baltic experienced multiple marine transgressions when the ongoing sea level rise outpaced glacioisostatic rebound (Björck et al., 2008). The mean sea level reached its highest level in the Baltic during the Littorina Sea stage (~7.5–~5 ka BP in Berglund et al., 2005). The water depth in the Little Belt increased considerably (~5–8 m) during these transgressions (Berglund et al., 2005), which led to a significant increase in North Sea water inflows due to deeper sills and straits. The Baltic Sea salinity increase during this stage may therefore be a result of the sea level rise and the increased cross-sectional area in the Danish Straits, permitting increased inflow of marine water from the Kattegat (Westman et al., 1999), which would likely apply to the Little Belt as well. The high salinity in the Little Belt may also be related to reduced brackish water outflow from the Baltic Sea between 6.2 and 4.7 ka BP (Gyllencreutz et al., 2006). The transgressions continued but were less extensive in the southernmost Baltic after 6 ka BP, while in the central and northern Baltic, the uplift was still ongoing, resulting in a renewed regression in the central Baltic (Björck et al., 2008). During the late Littorina Sea stage, mean sea level of southern Baltic coastal area steadily fell until reaching present day sea level (Berglund et al., 2005).

We compare our data with the inferred NAO circulation pattern over the past 5.2 kyr in order to test a link between water exchange through the Little Belt and the NAO on longer time scales. Reconstructions of the NAO index are based on tree rings and speleothem data (Trouet et al., 2009), as well as high resolution lake sediment geochemistry (Olsen et al., 2012). Principal component analysis 3 (PCA3) was used in Olsen et al. (2012) to integrate the redox variability (palaeo-redox proxy: Mn/Fe ratio), which can be associated with NAO-like atmospheric circulation patterns (Olsen et al., 2012). PCA3-inferred NAO patterns (Figure 6f) show that the NAO changed to variable and intermittently negative conditions during the time interval 4.3–~2 ka BP, coinciding with the temperature and salinity decreases documented in the Little Belt. The salinity decrease during this period may likely be ascribed to both a sea level drop in the Baltic Sea and often negative NAO conditions, following intermittent positive NAO phases. A similar positive correlation between NAO and sea level in the Skagerrak and Kattegat was also observed for the time period 1955–2000 by Wakelin et al. (2003).

During the generally negative NAO phase (4.3–~2 ka BP), the water depth decreased due to a sea level drop in the Little Belt, which led to a salinity decrease (Figures 6d–6f) due to fewer inflows from the North Sea and more brackish water in the region. Meanwhile, oxygen conditions improved when salinity decreased in the Baltic Sea during this period as the halocline was relatively deeper and stratification was weaker in the water column (Gerlach, 1994). However, the sea level variability was less likely to have made substantial contributions to the temperature variations in the Little Belt as the shallower water coincided with bottom water temperature decrease during 4.3–2 ka BP.

From ~2–0.5 ka BP, a continuous positive NAO phase led to a milder and less variable Baltic Sea climate compared to the previous period with intermittently negative and positive NAO conditions. The water depth and the bottom water conditions in the Little Belt became more stable. It should be noted that the various NAO reconstructions show somewhat different results (Nesje et al., 2000; Olsen et al., 2012), and consequently, we only focus on the general patterns where the various NAO reconstructions are largely similar. Both NAO reconstructions indicate that the NAO index was variable and intermittently negative in the mid-late Holocene, which coincides with the period of variable water conditions (Figure S7). The relative abundance of *E. incertum* and the Shannon diversity index are positively correlated with NAO (both $p < 0.01$) reconstructed by Nesje et al. (2000) (Figure S7).

5.2. Oxygen Reconstruction

Generally, the increasing trend of foraminiferal $\delta^{13}C_c$ and the decreasing trend of foraminiferal Mn/Ca (Figure 5f) suggest that the bottom water in the Little Belt became less stratified and more ventilated and therefore more oxygenated over time. Bottom water exchange and renewal can result in rapid increases of

the $\delta^{13}C_{DIC}$ (e.g., Filipsson et al., 2017) and significantly alter the $\delta^{13}C$ signal in foraminiferal carbonate. The $\delta^{18}O_c$ and $\delta^{13}C_c$ data show a weak but significant positive correlation ($r^2 = 0.14$, $p < 0.01$); this correlation presumably indicates changes in water mass composition, as a new water mass would usually be associated with changes in $\delta^{18}O_{water}$ and $\delta^{13}C_{DIC}$ (Filipsson et al., 2017). Moreover, more negative $\delta^{13}C_c$ values during LB1 and LB2 (Figure 6g) indicate higher primary productivity and more organic matter deposition, which may cause oxygen depletion and therefore hypoxia. The relatively positive $\delta^{13}C_c$ in LB3 most likely indicates lower productivity and more oxygenated bottom water conditions.

High foraminiferal Mn/Ca in zone LB1 and LB2 (7.5–3.3 ka BP) suggests hypoxic conditions during these intervals, which coincide with the HTM in the Baltic region (Zillén et al., 2008). The hypoxic periods in the Little Belt overlap in time with hypoxic events in the Baltic Proper, as indicated by C_{org}/P_{tot} and sediment lamination and bioturbation intervals (Jilbert & Slomp, 2013; Zillén et al., 2008). In the most recent stage LB3 (~3–0.8 ka BP), Mg/Ca and Mn/Ca in foraminiferal calcite are similar to modern calibration values of benthic foraminifera (Groeneveld et al., 2018) (see stars in Figures 4a–4c). Foraminiferal Mg/Ca and Mn/Ca show a relatively warm period with low bottom water oxygen content from 7.5 to 6.8 ka and from 5.3 to 3.3 ka BP. Significant positive correlation between foraminiferal Mg/Ca and Mn/Ca ratios ($r^2 = 0.73$, $p < 0.01$) suggests a strong interaction between temperature and dissolved $[O_2]$ in the bottom water, which is supported by modern hydrological correlation between bottom water temperature and dissolved oxygen concentration. However, there are also significant correlations between Ba/Ca and Mg/Ca and Ba/Ca and Mn/Ca. Solution-based TE/Ca measurements (Kotthoff et al., 2017) show similar TE/Ca results compared to the ones measured by LA-ICP-MS (Figure S1). We cannot completely exclude some potential contaminations of authigenic carbonate minerals inside the pores or that authigenic carbonates have replaced some primary calcite in some samples that cannot be removed by using LA profiles or standard cleaning procedures. To assess this, we compare our oxygen proxy results to the study of Site M0059 by van Helmond et al. (2017), which used bulk sediment geochemistry to evaluate past hypoxia in the Little Belt. They concluded that the presence of hypoxia is indicated by elevated Fe-carbonate concentrations (Fe_{carb}) in the bulk sediments in the time interval ~7–2.5 ka BP and after ~1 ka BP. In addition, the bulk sediment molybdenum (Mo) concentrations at Site M0059 suggest that (seasonal) hypoxia occurred continuously after the Ancylus/Littorina transition. In general, their bulk sediment hypoxia indicators agree with our oxygen proxies, providing support for our results.

5.3. Modern Hydrographical Setting versus NAO

The observed salinity variations of surface waters in the modern hydrographical data from the Little Belt (Figure 2c) can be explained by the seasonality of freshwater input, as surface water salinity is directly affected by river inflow and precipitation. However, the bottom water masses are more complex in such a shallow transitional area. In addition to river inflow and precipitation, the bottom water is also strongly affected by inflow of saline and oxygenated water from the North Sea, with the water inflow in the Little Belt generally being strong and highly turbulent, causing distinct vertical mixing (Jakobsen & Ottavi, 1997). Therefore, the stratification is often not very strong in the Little Belt compared to the Baltic Proper, but the pycnocline is still comparatively stronger during summer due to the increased freshwater influx and summer heating of surface waters, resulting in an increased temperature and salinity difference between surface and bottom waters. Both annual and monthly mean bottom water temperature and oxygen concentration over a 20-year period (1989–2018) show significant inverse correlation ($r^2 = 0.29$, $p = 0.002$; $r^2 = 0.59$, $p \ll 0.01$, respectively) (Table S1). This reveals that the dissolved bottom water $[O_2]$ decreases as water temperature increases (also seen in Figure 2). We applied these correlations to our past reconstructed bottom water salinity, temperature and dissolved $[O_2]$ with the reconstructed NAO index (Olsen et al., 2012), with the limitations in mind, aiming to investigate the mechanisms behind the environmental condition changes in the past. This inverse correlation is similar to that we have observed in reconstructed temperature and oxygen conditions in the bottom water in the Little Belt over the past 7.5 kyr.

The correlation between the winter-NAO index (Jones et al., 1997) and winter bottom water salinity from instrumental data (Baltic Nest, http://nest.su.se) is weak but significant ($r^2 = 0.12$, $p = 0.036$) (Table S2), presumably due to the profound effect of NAO on winter climate in the region. However, no significant correlation is seen between monthly mean bottom water salinity and the NAO index, and there is no significant linear correlation between the winter NAO and temperature or oxygen concentration of deep water in the

past four decades. The positive correlation is also observed in reconstructed bottom water salinity and reconstructed NAO index (Olsen et al., 2012).

The winter NAO has a significantly positive influence on the inflow of saline water and therefore on the bottom water salinity, that is, higher salinities occur in the straits during winters with less wind from the north and northeast. However, the transport of water (and thereby indirectly salinity) in the Danish Straits is also to a large degree controlled by the short-term variability in relative sea level (Jakobsen et al., 2010), a variability that we do not register with the above analyses. Several studies suggest a NAO impact on Baltic sea level variations and demonstrate a high correlation between winter NAO index and the Baltic Sea and Kattegat winter mean sea level (e.g.,Andersson, 2002 ; Kuijpers et al., 2012 ; Różyński, 2015 ; Wakelin et al., 2003). Water depth variations attributed to North Atlantic atmospheric circulation further influence the bottom water salinity and bottom water circulation.

6. Conclusion

By combining the foraminiferal trace elemental, isotopic, and faunal assemblage data with pore water $\delta^{18}O$ data, we have quantitatively reconstructed bottom water temperature, salinity and oxygenation at the entrance to the Baltic Sea since 7.7 ka, making it possible to evaluate the link between overall climatic conditions, water mass exchange and bottom-water hypoxia.

At the start of our record (the beginning of the brackish-marine Littorina Sea stage) between 7.7 and 7.5 ka BP, salinity increased markedly from ~24 to ~30. The bottom water temperature, the dissolved $[O_2]$ and the primary production varied between 7.5 and ~6.8 ka BP, indicating intensive environmental changes in this entrance area to the Baltic Sea. Relatively warmer and more saline bottom water conditions developed between 6 and 3 ka BP, that is, the main Littorina Sea stage. Meanwhile, primary productivity became high, and combined with increased stratification, this caused hypoxia in the bottom water in the Little Belt. The period with high bottom water temperature and salinity and low dissolved $[O_2]$ (7.5–3.3 ka BP) coincides in time with the HTM and with transgression and high sea level, and greater water depth in the Little Belt. After the HTM, salinity and temperature decreased in the time interval ~4.1–2.5 ka BP, coinciding with variable and intermittently negative NAO index. This was followed since 2.5 ka BP by cooler and fresher bottom water conditions until the present. The bottom water temperature decreased ~7 °C, while the salinity decreased six units between 4.1 and 2.5 ka BP. The salinity decrease after 4.1 ka BP can be recognized by modeled pore water $\delta^{18}O$ results, but cannot be seen independently in foraminiferal $\delta^{18}O_c$ and Ba/Ca data. However, when $\delta^{18}O_c$ and Mg/Ca data are combined to calculate salinity, a similar decrease is observed. The different temperature proxies used in this study (foraminiferal Mg/Ca and $\delta^{18}O$) show similar trends over the past 7.5 kyr with an absolute temperature difference of about ~1 °C.

Modern bottom water salinity in the Little Belt and winter NAO index show a significant positive correlation. A similar, but somewhat weaker correlation is seen in our paleorecord, where temperature and salinity of the bottom waters decreased during intermittently negative NAO phase (4.3–~2 ka BP). In addition, the salinity decrease at ~4 ka BP may also be linked to a well-known regional glacio-isostatic sea-level fall during the late Littorina Sea stage. Broadly, more oxygenated bottom water conditions in the past 4 kyr are likely caused by a combination of shallower water depth, and lower temperature and salinity. Our multiproxy record demonstrates that the changes in bottom water conditions at the boundary between the brackish Baltic Proper and marine Kattegat/North Sea are noticeably influenced by larger scale climate and topographical change (i.e., NAO and eustatic sea level), and they are also linked to the changes in the other parts of the Baltic Sea.

References

Andersson, H. C. (2002). Influence of long-term regional and large-scale atmospheric circulation on the Baltic sea level. *Tellus Series A: Dynamic Meteorology and Oceanography*, *54*(1), 76–88. https://doi.org/10.1034/j.1600-0870.2002.00288.x

Andrén, T., Björck, S., Andrén, E., Conley, D., Zillén, L., & Anjar, J. (2011). The development of the Baltic Sea Basin during the last 130 ka. In J. Harff, S. Björck, & P. Hoth (Eds.), *The Baltic Sea Basin* (pp. 75–97). Berlin, Heidelberg: Springer.

Andrén, T., Jørgensen, B. B., Cotterill, C., Green, S., & IODP Expedition 347 Scientific Party (2015). Baltic Sea basin paleoenvironment and biosphere. *Scientific Drilling*, *20*, 1–12. https://doi.org/10.5194/sd-20-1-2015

Barrientos, N., Lear, C. H., Jakobsson, M., Stranne, C., O'Regan, M., Cronin, T. M., et al. (2018). Arctic Ocean benthic foraminifera Mg/Ca ratios and global Mg/Ca-temperature calibrations: New constraints at low temperatures. *Geochimica et Cosmochimica Acta*, *236*, 240–259. https://doi.org/10.1016/j.gca.2018.02.036

Bathmann, U., Dutschke, F., Glockzin, M., Gogina, M., Lipka, M., Naderipour, C., et al. (2017). Coastal benthic environments in North and Baltic Sea: Evaluation of processes and transports at the sediment-water interface (Küno INTERFACE). Maria S. Merian-Berichte, MSM50, 50 pp., DFG-Senatskommission für Ozeanographie. https://doi.org/10.2312/cr_msm50

Bennike, O., & Jensen, J. B. (2011). Postglacial, relative shore-level changes in Lillebælt, Denmark. *Geological Survey of Denmark and Greenland Bulletin*, *23*, 37–40. https://doi.org/10.1111/j.1502-3885.2010.00180.x

Berglund, B. E., Sandgren, P., Barnekow, L., Hannon, G., Jiang, H., Skog, G., & Yu, S.-Y. (2005). Early Holocene history of the Baltic Sea, as reflected in coastal sediments in Blekinge, southeastern Sweden. *Quaternary International*, *130*(1), 111–139. https://doi.org/10.1016/j.quaint.2004.04.036

Berner, R. A. (1980). *Early diagenesis: A theoretical approach*. Princeton, NJ: Princeton University Press. https://doi.org/10.1002/gj.3350160113

Björck, S., Andrén, T., & Jensen, J. B. (2008). An attempt to resolve the partly conflicting data and ideas on the Ancylus-Littorina transition. *Polish Geological Institute Special Papers*, *23*, 21–26.

Böttcher, M. E., & Dietzel, M. (2010). Metal-ion partitioning during low-temperature precipitation and dissolution of anhydrous carbonates and sulphates. *European Mineralogical Union Notes in Mineralogy*, *10*(1), 139–187. https://doi.org/10.1180/EMU-notes.10.4

Böttcher, M. E., & Lepland, A. (2000). Biogeochemistry of sulfur in a sediment core from the west-central Baltic Sea: Evidence from stable isotopes and pyrite textures. *Journal of Marine Systems*, *25*(3-4), 299–312. https://doi.org/10.1016/S0924-7963(00)00023-3

Böttcher, M. E., Lipka, M., Winde, V., Dellwig, O., Böttcher, E. O., Böttcher, T., & Schmiedinger, I. (2014). Multi-isotope composition of freshwater sources for the southern North and Baltic Sea. In H. Wiederhold, J. Michaelsen, & B. Hinsby (Eds.), *SWIM 2014, 23rd Salt Water Intrusion Meeting, June 16-20, 2014, Husum, Germany, programme and proceedings* (pp. 46–49). Hannover: Leibniz-Institut für Angewandte Geophysik. ISBN: 978-3-00-046061-6.

Boudreau, B. P. (1996). The diffusive tortuosity of fine-grained unlithified sediments. *Geochimica et Cosmochimica Acta*, *60*(16), 3139–3142. https://doi.org/10.1016/0016-7037(96)00158-5

Boudreau, B. P. (1997). *Diagenetic models and their implementation* (Vol. 505). Berlin: Springer. https://doi.org/10.1007/978-3-642-60421-8

Boyle, E. A. (1983). Manganese carbonate overgrowths on foraminifera tests. *Geochimica et Cosmochimica Acta*, *47*(10), 1815–1819. https://doi.org/10.1016/0016-7037(83)90029-7

Breitburg, D. (2002). Effects of hypoxia, and the balance between hypoxia and enrichment, on coastal fishes and fisheries. *Estuaries*, *25*(4), 767–781. https://doi.org/10.1007/BF02804904

Carstensen, J., Andersen, J. H., Gustafsson, B. G., & Conley, D. J. (2014). Deoxygenation of the Baltic Sea during the last century. *Proceedings of the National Academy of Sciences*, *111*(15), 5628–5633. https://doi.org/10.1073/pnas.1323156111

Charrieau, L. M., Filipsson, H. L., Ljung, K., Chierici, M., Knudsen, K. L., & Kritzberg, E. (2018). The effects of multiple stressors on the distribution of coastal benthic foraminifera: A case study from the Skagerrak-Baltic Sea region. *Marine Micropaleontology*, *139*, 42–56. https://doi.org/10.1016/j.marmicro.2017.11.004

Charrieau, L. M., Ljung, K., Schenk, F., Daewel, U., Kritzberg, E., & Filipsson, H. L. (2019). Rapid environmental responses to climate-induced hydrographic changes in the Baltic Sea entrance. *Biogeosciences*, *16*(19), 3835–3852. https://doi.org/10.5194/bg-16-3835-2019

Conley, D. J., Carstensen, J., Aigars, J., Axe, P., Bonsdorff, E., Eremina, T., et al. (2011). Hypoxia is increasing in the coastal zone of the Baltic Sea. *Environmental Science & Technology*, *45*(16), 6777–6783. https://doi.org/10.1021/es201212r

Conley, D. J., Carstensen, J., Vaquer-Sunyer, R., & Duarte, C. M. (2009). Ecosystem thresholds with hypoxia. *Hydrobiologia*, *629*, 21–29. https://doi.org/10.1007/978-90-481-3385-7_3

Conradsen, K., Bergsten, H., Knudsen, K. L., Nordberg, K., & Seidenkrantz, M. (1994). Recent benthic foraminiferal distribution in the Kattegat and the Skagerrak, Scandinavia. *Cushman Foundation for Foraminiferal Research, Special Publication*, *32*, 53–68.

Diaz, R. J., & Rosenberg, R. (2008). Spreading dead zones and consequences for marine ecosystems. *Science*, *321*(5891), 926–929. https://doi.org/10.1126/science.1156401

Dueñas-Bohórquez, A., Raitzsch, M., de Nooijer, L. J., & Reichart, G.-J. (2011). Independent impacts of calcium and carbonate ion concentration on Mg and Sr incorporation in cultured benthic foraminifera. *Marine Micropaleontology*, *81*(3-4), 122–130. https://doi.org/10.1016/j.marmicro.2011.08.002

Egger, M., Hagens, M., Sapart, C. J., Dijkstra, N., van Helmond, N. A., Mogollón, J. M., et al. (2017). Iron oxide reduction in methane-rich deep Baltic Sea sediments. *Geochimica et Cosmochimica Acta*, *207*, 256–276. https://doi.org/10.1016/j.gca.2017.03.019

Elderfield, H., Greaves, M., Barker, S., Hall, I. R., Tripati, A., Ferretti, P., et al. (2010). A record of bottom water temperature and seawater $\delta^{18}O$ for the Southern Ocean over the past 440 kyr based on Mg/Ca of benthic foraminiferal *Uvigerina spp*. *Quaternary Science Reviews*, *29*(1-2), 160–169. https://doi.org/10.1016/j.quascirev.2009.07.013

Elderfield, H., Yu, J., Anand, P., Kiefer, T., & Nyland, B. (2006). Calibrations for benthic foraminiferal Mg/Ca paleothermometry and the carbonate ion hypothesis. *Earth and Planetary Science Letters*, *250*(3-4), 633–649. https://doi.org/10.1016/j.epsl.2006.07.041

Emeis, K.-C., Struck, U., Blanz, T., Kohly, A., & Voβ, M. (2003). Salinity changes in the central Baltic Sea (NW Europe) over the last 10000 years. *The Holocene*, *13*(3), 411–421. https://doi.org/10.1191/0959683603hl634rp

Feyling-Hanssen, R. W. (1972). The foraminifer *Elphidium excavatum* (Terquem) and its variant forms. *Micropaleontology*, *18*, 337–354. https://www.jstor.org/stable/1485012

Feyling-Hanssen, R. W., Jørgensen, J. A., Knudsen, K. L., & Lykke-Andersen, A.-L. (1971). Late quaternary foraminifera from Vendsyssel, Denmark and Sandnes, Norway. *Bulletin of the Geological Society of Denmark*, *21*(2-3), 67–317.

Filipsson, H. L., Bernhard, J. M., Lincoln, S. A., & McCorkle, D. C. (2010). A culture-based calibration of benthic foraminiferal paleo-temperature proxies: delta O-18 and Mg/Ca results. *Biogeosciences*, *7*, 1335–1347. https://doi.org/10.5194/bg-7-1335-2010

Filipsson, H. L., McCorkle, D. C., Mackensen, A., Bernhard, J. M., Andersson, L. S., Naustvoll, L.-J., et al. (2017). Seasonal variability of stable carbon isotopes ($\delta^{13}C_{DIC}$) in the Skagerrak and the Baltic Sea: Distinguishing between mixing and biological productivity. *Palaeogeography, Palaeoclimatology, Palaeoecology*, *483*, 15–30. https://doi.org/10.1016/j.palaeo.2016.11.031

Filipsson, H. L., & Nordberg, K. (2010). Variations in organic carbon flux and stagnation periods during the last 2400 years in a Skagerrak fjord basin, inferred from benthic foraminiferal $\delta^{13}C$. *Geological Society, London, Special Publications*, *344*(1), 261–270. https://doi.org/10.1144/SP344.18

Fischer, H., & Matthäus, W. (1996). The importance of the Drogden Sill in the Sound for major Baltic inflows. *Journal of Marine Systems*, *9*(3-4), 137–157. https://doi.org/10.1016/S0924-7963(96)00046-2

Fröhlich, K., Grabczak, J., & Rozanski, K. (1988). Deuterium and oxygen-18 in the Baltic Sea. *Chemical Geology: Isotope Geoscience*, *72*(1), 77–83. https://doi.org/10.1016/0168-9622(88)90038-3

Gat, J. R. (1996). Oxygen and hydrogen isotopes in the hydrologic cycle. *Annual Review of Earth and Planetary Sciences*, *24*(1), 225–262. https://doi.org/10.1146/annurev.earth.24.1.225

Gerlach, S. A. (1994). Oxygen conditions improve when the salinity in the Baltic Sea decreases. *Marine Pollution Bulletin*, *28*(7), 413–416. https://doi.org/10.1016/0025-326X(94)90126-0

Glock, N., Eisenhauer, A., Liebetrau, V., Wiedenbeck, M., Hensen, C., & Nehrke, G. (2012). EMP and SIMS studies on Mn/Ca and Fe/Ca systematics in benthic foraminifera from the Peruvian OMZ: A contribution to the identification of potential redox proxies and the impact of cleaning protocols. *Biogeosciences*, *9*(1), 341–359. https://doi.org/10.5194/bg-9-341-2012

Godhe, A., & McQuoid, M. R. (2003). Influence of benthic and pelagic environmental factors on the distribution of dinoflagellate cysts in surface sediments along the Swedish west coast. *Aquatic Microbial Ecology*, *32*(2), 185–201. https://doi.org/10.3354/ame032185

Groeneveld, J., & Filipsson, H. (2013). Mg/Ca and Mn/Ca ratios in benthic foraminifera: The potential to reconstruct past variations in temperature and hypoxia in shelf regions. *Biogeosciences*, *10*(7), 5125–5138. https://doi.org/10.5194/bg-10-5125-2013

Groeneveld, J., Filipsson, H. L., Austin, W. E., Darling, K., McCarthy, D., Krupinski, N. B. Q., et al. (2018). Assessing proxy signatures of temperature, salinity, and hypoxia in the Baltic Sea through foraminifera-based geochemistry and faunal assemblages. *Journal of Micropalaeontology*, *37*(2), 403–429. https://doi.org/10.5194/jm-37-403-20

Gustafsson, B. G., & Westman, P. (2002). On the causes for salinity variations in the Baltic Sea during the last 8500 years. *Paleoceanography*, *17*(3), 1040. https://doi.org/10.1029/2000PA000572

Gustafsson, M., & Nordberg, K. (2001). Living (stained) benthic foraminiferal response to primary production and hydrography in the deepest part of the Gullmar Fjord, Swedish West Coast, with comparisons to Hoglund's 1927 material. *Journal of Foraminiferal Research*, *31*(1), 2–11. https://doi.org/10.2113/0310002

Gyllencreutz, R., Backman, J., Jakobsson, M., Kissel, C., & Arnold, E. (2006). Postglacial palaeoceanography in the Skagerrak. *The Holocene*, *16*(7), 975–985. https://doi.org/10.1177/0959683606hl988rp

Hänninen, J., Vuorinen, I., & Hjelt, P. (2000). Climatic factors in the Atlantic control the oceanographic and ecological changes in the Baltic Sea. *Limnology and Oceanography*, *45*(3), 703–710. https://doi.org/10.4319/lo.2000.45.3.0703

Harwood, A. J., Dennis, P. F., Marca, A. D., Pilling, G. M., & Millner, R. S. (2008). The oxygen isotope composition of water masses within the North Sea. *Estuarine, Coastal and Shelf Science*, *78*(2), 353–359. https://doi.org/10.1016/j.ecss.2007.12.010

Hathorne, E. C., James, R. H., Savage, P., & Alard, O. (2008). Physical and chemical characteristics of particles produced by laser ablation of biogenic calcium carbonate. *Journal of Analytical Atomic Spectrometry*, *23*(2), 240–243. https://doi.org/10.1039/b706727e

Hayward, B. W., Holzmann, M., & Tsuchiya, M. (2019). Combined molecular and morphological taxonomy of the Beccarii/T3 group of the foraminiferal genus ammonia. *Journal of Foraminiferal Research*, *49*(4), 367–389. https://doi.org/10.2113/gsjfr.49.4.367

Hela, I. (1944). Uber die Schwankungen des Wasserstandes in der Ostsee mit besonderer BerUcksichtigung des Wasseraustausches durch die danischen Gewässer. Merentutkimuslaitoksen Julkaisu Havsforskningsinstitutets Skrift, N 134, Helsinki, 1-108.

Helsinki Commission (HELCOM). (1986). Water balance of the Baltic Sea. Baltic Sea Environmental Proceedings, 16, 179.

Hönisch, B., Allen, K. A., Russell, A. D., Eggins, S. M., Bijma, J., Spero, H. J., et al. (2011). Planktic foraminifers as recorders of seawater Ba/Ca. *Marine Micropaleontology*, *79*(1-2), 52–57. https://doi.org/10.1016/j.marmicro.2011.01.003

Hurrell, J. W. (1995). Decadal trends in the North Atlantic Oscillation: Regional temperatures and precipitation. *Science*, *269*(5224), 676–679. https://doi.org/10.1126/science.269.5224.676

Hurrell, J. W. (1996). Influence of variations in extratropical wintertime teleconnections on Northern Hemisphere temperature. *Geophysical Research Letters*, *23*(6), 665–668. https://doi.org/10.1029/96GL00459

Hurrell, J. W., Kushnir, Y., Ottersen, G., & Visbeck, M. (2003). *An overview of the North Atlantic oscillation*, *Geophysical Monograph* (Vol. 134, pp. 1–36). Washington, DC: American Geophysical Union. https://doi.org/10.1029/134GM01

International Council for the Exploration of the Sea (ICES) (2018). Baltic Sea ecoregion—Ecosystem overview, 1-25. https://doi.org/10.17895/ices.pub.4665

Jacobsen, T. S. (1980). Sea water exchange of the Baltic. Measurements and methods. The Belt Project, The National Agency of Environmental Protection, 106 pp.

Jakobsen, F. (1995). The major inflow to the Baltic Sea during January 1993. *Journal of Marine Systems*, *6*(3), 227–240. https://doi.org/10.1016/0924-7963(94)00025-7

Jakobsen, F., Hansen, I. S., Hansen, N. E. O., & Østrup-Rasmussen, F. (2010). Flow resistance in the Great Belt, the biggest strait between the North Sea and the Baltic Sea. *Estuarine, Coastal and Shelf Science*, *87*(2), 325–332. https://doi.org/10.1016/j.ecss.2010.01.014

Jakobsen, F., & Ottavi, J. (1997). Transport through the contraction area in the Little Belt. *Estuarine, Coastal and Shelf Science*, *45*(6), 759–767. https://doi.org/10.1006/ecss.1997.0238

Jilbert, T., & Slomp, C. P. (2013). Rapid high-amplitude variability in Baltic Sea hypoxia during the Holocene. *Geology*, *41*(11), 1183–1186. https://doi.org/10.1130/G34804.1

Jochum, K. P., Scholz, D., Stoll, B., Weis, U., Wilson, S. A., Yang, Q., et al. (2012). Accurate trace element analysis of speleothems and biogenic calcium carbonates by LA-ICP-MS. *Chemical Geology*, *318-319*, 31–44. https://doi.org/10.1016/j.chemgeo.2012.05.009

Jochum, K. P., Weis, U., Stoll, B., Kuzmin, D., Yang, Q., Raczek, I., et al. (2011). Determination of reference values for NIST SRM 610–617 glasses following ISO guidelines. *Geostandards and Geoanalytical Research*, *35*(4), 397–429. https://doi.org/10.1111/j.1751-908X.2011.00120.x

Johansson, M., Boman, H., Kahma, K. K., & Launiainen, J. (2001). Trends in sea level variability in the Baltic Sea. *Boreal Environment Research*, *6*(3), 159–180.

Johansson, M. M., Kahma, K. K., & Boman, H. (2003). An improved estimate for the long-term mean sea level on the Finnish coast. *Geophysica*, *39*(1-2), 51–73.

Jones, P. D., Jonsson, T., & Wheeler, D. (1997). Extension to the North Atlantic Oscillation using early instrumental pressure observations from Gibralter and south-west Iceland. *International Journal of Climatology*, *17*(13), 1433–1450. https://doi.org/10.1002/(SICI)1097-0088(19971115)17:13<1433::AID-JOC203>3.0.CO;2-P

Kabel, K., Moros, M., Porsche, C., Neumann, T., Adolphi, F., Andersen, T. J., et al. (2012). Impact of climate change on the Baltic Sea ecosystem over the past 1,000 years. *Nature Climate Change*, *2*(12), 871. https://doi.org/10.1038/nclimate1595

Katz, M. E., Cramer, B. S., Franzese, A., Hönisch, B. R., Miller, K. G., Rosenthal, Y., & Wright, J. D. (2010). Traditional and emerging geochemical proxies in foraminifera. *Journal of Foraminiferal Research*, *40*(2), 165–192. https://doi.org/10.2113/gsjfr.40.2.165

Koho, K., de Nooijer, L., & Reichart, G. (2015). Combining benthic foraminiferal ecology and shell Mn/Ca to deconvolve past bottom water oxygenation and paleoproductivity. *Geochimica et Cosmochimica Acta*, *165*, 294–306. https://doi.org/10.1016/j.gca.2015.06.003

Koho, K. A., de Nooijer, L. J., Fontanier, C., Toyofuku, T., Oguri, K., Kitazato, H., & Reichart, G.-J. (2017). Benthic foraminiferal Mn/Ca ratios reflect microhabitat preferences. *Biogeosciences*, *14*(12), 3067–3082. https://doi.org/10.5194/bg-14-3067-2017

Kotthoff, U., Groeneveld, J., Ash, J., Fanget, A.-S., Krupinski, N. Q., Peyron, O., et al. (2017). Reconstructing Holocene temperature and salinity variations in the western Baltic Sea region: A multi-proxy comparison from the Little Belt (IODP Expedition 347, Site M0059). *Biogeosciences*, *14*(23), 5607–5632. https://doi.org/10.5194/bg-14-5607-2017

Kristjánsdóttir, G., Lea, D., Jennings, A., Pak, D., & Belanger, C. (2007). New spatial Mg/Ca-temperature calibrations for three Arctic, benthic foraminifera and reconstruction of north Iceland shelf temperature for the past 4000 years. *Geochemistry, Geophysics, Geosystems*, *8*, Q03P21. https://doi.org/10.1029/2006GC001425

Kuijpers, A., Kunzendorf, H., Rasmussen, P., Sicre, M. A., Ezat, U., Fernane, A., & Weckström, K. (2012). The Baltic Sea inflow regime at the termination of the Medieval Climate Anomaly linked to North Atlantic circulation. *Baltica*, *25*(1), 57–64. https://doi.org/10.5200/baltica.2012.25.05

Lambert, E., Eldevik, T., & Haugan, P. M. (2016). How northern freshwater input can stabilise thermohaline circulation. *Tellus A: Dynamic Meteorology and Oceanography*, *68*(1), p.31051. https://doi.org/10.3402/tellusa.v68.31051

Lambert, E., Eldevik, T., & Spall, M. A. (2018). On the dynamics and water mass transformation of a boundary current connecting alpha and beta oceans. *Journal of Physical Oceanography*, *48*(10), 2457–2475. https://doi.org/10.1175/JPO-D-17-0186.1

Lass, H. U., & Matthäus, W. (2008). General oceanography of the Baltic Sea. State and Evolution of the Baltic Sea, 1952–2005. In R. Feistel, G. Nausch, & N. Wasmund (Eds.), *A Detailed 50-Year Survey of Meteorology and Climate, Physics, Chemistry, Biology, and Marine Environment* (pp. 5–43). Hoboken, NJ: John Wiley & Sons, Inc. https://doi.org/10.1002/9780470283134.ch2

Lea, D., & Boyle, E. (1989). Barium content of benthic foraminifera controlled by bottom-water composition. *Nature*, *338*(6218), 751–753. https://doi.org/10.1038/338751a0

Lea, D. W., & Boyle, E. A. (1991). Barium in planktonic foraminifera. *Geochimica et Cosmochimica Acta*, *55*(11), 3321–3331. https://doi.org/10.1016/0016-7037(91)90491-M

LeGrande, A. N., & Schmidt, G. A. (2006). Global gridded data set of the oxygen isotopic composition in seawater. *Geophysical Research Letters*, *33*, L12604. https://doi.org/10.1029/2006GL026011

Lehmann, A., Höflich, K., Post, P., & Myrberg, K. (2017). Pathways of deep cyclones associated with large volume changes (LVCs) and major Baltic inflows (MBIs). *Journal of Marine Systems*, *167*, 11–18. https://doi.org/10.1016/j.jmarsys.2016.10.014

Lu, J., & Greatbatch, R. J. (2002). The changing relationship between the NAO and northern hemisphere climate variability. *Geophysical Research Letters*, *29*(7), 1148. https://doi.org/10.1029/2001GL014052

Marshall, J., Johnson, H., & Goodman, J. (2001). A study of the interaction of the North Atlantic Oscillation with ocean circulation. *Journal of Climate*, *14*(7), 1399–1421. https://doi.org/10.1175/1520-0442(2001)014<1399:ASOTIO>2.0.CO;2

Massel, S. R. (2015). *Internal gravity waves in the shallow seas*. Berlin: Springer. https://doi.org/10.1007/978-3-319-18908-6

Matthäus, W., & Franck, H. (1992). Characteristics of major Baltic inflows—A statistical analysis. *Continental Shelf Research*, *12*(12), 1375–1400. https://doi.org/10.1016/0278-4343(92)90060-W

Matthäus, W., Nehring, D., Feistel, R., Nausch, G., Mohrholz, V., & Lass, H. U. (2008). The inflow of highly saline water into the Baltic Sea. State and Evolution of the Baltic Sea, 1952–2005. In R. Feistel, G. Nausch, & N. Wasmund (Eds.), *A Detailed 50-Year Survey of Meteorology and Climate, Physics, Chemistry, Biology, and Marine Environment* (pp. 265–309). Hoboken, NJ: John Wiley & Sons, Inc. https://doi.org/10.1002/9780470283134.ch10

McKay, C., Groenevold, J., Filipsson, H., Gallego-Torres, D., Whitehouse, M. J., Toyofuku, T., & Romero, O. (2015). A comparison of benthic foraminiferal Mn/Ca and sedimentary Mn/Al as proxies of relative bottom-water oxygenation in the low-latitude NE Atlantic upwelling system. *Biogeosciences*, *12*, 5415–5428. https://doi.org/10.5194/bg-12-5415-2015

Mehta, V. M., Suarez, M. J., Manganello, J. V., & Delworth, T. L. (2000). Oceanic influence on the North Atlantic Oscillation and associated Northern Hemisphere climate variations: 1959–1993. *Geophysical Research Letters*, *27*(1), 121–124. https://doi.org/10.1029/1999GL002381

Meier, H. M., Broman, B., & Kjellström, E. (2004). Simulated sea level in past and future climates of the Baltic Sea. *Climate Research*, *27*(1), 59–75. https://doi.org/10.3354/cr027059

Murray, C. N., & Riley, J. P. (1969). The solubility of gases in distilled water and sea water-II. Oxygen. *Deep Sea Research*, *16*, 311–320.

Murray, J. W. (2006). *Ecology and applications of benthic foraminifera*. Cambridge: Cambridge University Press. https://doi.org/10.1017/CBO9780511535529

Nesje, A., Lie, Ø., & Dahl, S. O. (2000). Is the North Atlantic Oscillation reflected in Scandinavian glacier mass balance records? *Journal of Quaternary Science*, *15*(6), 587–601. https://doi.org/10.1002/1099-1417(200009)15:6<587::AID-JQS533>3.0.CO;2-2

Nilsson, S. (2006). International river basins in the Baltic Sea Region. BSR INTERREG III B Programme Project Report, 14. Retrieved from http://www.baltex-research.eu/material/downloads/riverbasins.pdf

Ning, W., Andersson, P. S., Ghosh, A., Khan, M., & Filipsson, H. L. (2017). Quantitative salinity reconstructions of the Baltic Sea during the mid-Holocene. *Boreas*, *46*(1), 100–110. https://doi.org/10.1111/bor.12156

Ning, W., Nielsen, A. B., Ivarsson, L. N., Jilbert, T., Åkesson, C. M., Slomp, C. P., et al. (2018). Anthropogenic and climatic impacts on a coastal environment in the Baltic Sea over the last 1000 years. *Anthropocene*, *21*, 66–79. https://doi.org/10.1016/j.ancene.2018.02.003

Olsen, J., Anderson, N. J., & Knudsen, M. F. (2012). Variability of the North Atlantic Oscillation over the past 5,200 years. *Nature Geoscience*, *5*(11), 808. https://doi.org/10.1038/NGEO1589

Pearson, P. N. (2012). Oxygen isotopes in foraminifera: Overview and historical review. *The Paleontological Society Papers*, *18*, 1–38. https://doi.org/10.1017/S1089332600002539

Polovodova Asteman, I., Filipsson, H. L., & Nordberg, K. (2018). Tracing winter temperatures over the last two millennia using a north-east Atlantic coastal record. *Climate of the Past*, *14*(7), 1097–1118. https://doi.org/10.5194/cp-14-1097-2018

Renssen, H., Seppä, H., Crosta, X., Goosse, H., & Roche, D. (2012). Global characterization of the Holocene thermal maximum. *Quaternary Science Reviews*, *48*, 7–19. https://doi.org/10.1016/j.quascirev.2012.05.022

Rohling, E. J., & Cooke, S. (1999). Stable oxygen and carbon isotopes in foraminiferal carbonate shells. In B. K. Sen Gupta (Ed.), *Modern foraminifera* (pp. 239–258). Dordrecht: Springer. https://doi.org/10.1007/0-306-48104-9_14

Różyński, G. (2015). Long term couplings of winter index of North Atlantic oscillation and water level in the Baltic Sea and Kattegat. *Ocean Engineering*, *109*, 113–126. https://doi.org/10.1016/j.oceaneng.2015.09.014

Schmiedl, G., & Mackensen, A. (2006). Multispecies stable isotopes of benthic foraminifers reveal past changes of organic matter decomposition and deepwater oxygenation in the Arabian Sea. *Paleoceanography*, *21*, PA4213. https://doi.org/10.1029/2006PA001284

Seidenkrantz, M.-S. (1993). Benthic foraminiferal and stable isotope evidence for a "Younger Dryas-style" cold spell at the Saalian-Eemian transition, Denmark. *Palaeogeography, Palaeoclimatology, Palaeoecology*, *102*(1-2), 103–120. https://doi.org/10.1016/0031-0182(93)90008-7

Shackleton, N. (1974). Attainment of isotopic equilibrium between ocean water and the benthonic foraminifera genus Uvigerina: Isotopic changes in the ocean during the last glacial. *Colloquium International, National Centre for Scientific Research*, *219*, 203–209.

Sohlenius, G., Emeis, K.-C., Andrén, E., Andrén, T., & Kohly, A. (2001). Development of anoxia during the Holocene fresh-brackish water transition in the Baltic Sea. *Marine Geology*, *177*(3-4), 221–242. https://doi.org/10.1016/S0025-3227(01)00174-8

Stepanova, A., Obrochta, S., Quintana Krupinski, N. B., Hyttinen, O., Kotilainen, A., & Andrén, T. (2019). Late Weichselian to Holocene history of the Baltic Sea as reflected in ostracod assemblages. *Boreas*, *48*(3), 761–778. https://doi.org/10.1111/bor.12375

Trigo, R. M., Osborn, T. J., & Corte-Real, J. M. (2002). The North Atlantic Oscillation influence on Europe: Climate impacts and associated physical mechanisms. *Climate Research*, *20*(1), 9–17. https://doi.org/10.3354/cr020009

Trouet, V., Esper, J., Graham, N. E., Baker, A., Scourse, J. D., & Frank, D. C. (2009). Persistent positive North Atlantic Oscillation mode dominated the medieval climate anomaly. *Science*, *324*(5923), 78–80. https://doi.org/10.1126/science.1166349

UNESCO, I. (1981). Tenth report of the joint panel on oceanographic tables and standards. UNESCO *Technical Papers Marine Science*, 36, 1-25.

van Helmond, N. A., Krupinski, N. B. Q., Lougheed, B. C., Obrochta, S. P., Andrén, T., & Slomp, C. P. (2017). Seasonal hypoxia was a natural feature of the coastal zone in the Little Belt, Denmark, during the past 8 ka. *Marine Geology*, *387*, 45–57. https://doi.org/10.1016/j.margeo.2017.03.008

van Wirdum, F., Andrén, E., Wienholz, D., Kotthoff, U., Moros, M., Fanget, A.-S., et al. (2019). Middle to late Holocene variations in salinity and primary productivity in the central Baltic Sea: A multiproxy study from the Landsort Deep. *Frontiers in Marine Science*, *6*, 51. https://doi.org/10.3389/fmars.2019.00051

Vetter, L., Spero, H. J., Russell, A. D., & Fehrenbacher, J. S. (2013). LA-ICP-MS depth profiling perspective on cleaning protocols for elemental analyses in planktic foraminifers. *Geochemistry, Geophysics, Geosystems*, *14*, 2916–2931. https://doi.org/10.1002/ggge.20163

von Bröckel, K., Wlost, K.-P., Maggiulli, M. & Riedel, F. (2018). "Maria S. Merian" research vessel manual, (Briese Research Forschungsschiffahrt (ed.)), 181 pp. Retrieved from https://www.ldf.uni-hamburg.de/en/merian/technisches/dokumente-tech-merian/handbuch-merian-eng.pdf

Wakelin, S., Woodworth, P., Flather, R., & Williams, J. (2003). Sea-level dependence on the NAO over the NW European Continental Shelf. *Geophysical Research Letters*, *30*(7), 1403. https://doi.org/10.1029/2003GL017041

Westman, P., Wastegård, S., Schoning, K., Gustafsson, B., & Omstedt, A. (1999). Salinity change in the Baltic Sea during the last 8,500 years: Evidence, causes and models. Swedish Nuclear Fuel and Waste Management Co., *Technical Report*, TR-- 99-38, 1-47.

Winsor, P., Rodhe, J., & Omstedt, A. (2001). Baltic Sea ocean climate: An analysis of 100 yr of hydrographic data with focus on the freshwater budget. *Climate Research*, *18*(1-2), 5–15. https://doi.org/10.3354/cr018005

Zillén, L., Conley, D. J., Andrén, T., Andrén, E., & Björck, S. (2008). Past occurrences of hypoxia in the Baltic Sea and the role of climate variability, environmental change and human impact. *Earth-Science Reviews*, *91*(1-4), 77–92. https://doi.org/10.1016/j.earscirev.2008.10.001